

TNO report**TNO 2015 R11538****JIP Experimental foam selection - Modelling of
foam pipe flow**

Leeghwaterstraat 44
2628 CA Delft
P.O. Box 6012
2600 JA Delft
The Netherlands

www.tno.nl

T +31 88 866 22 00

Date	17 December 2015
Author(s)	Jos van 't Westende Jordy de Boer Frank Vercauteren
Copy no	0100291545
Number of pages	81 (incl. appendices)
Project number	060.04189

All rights reserved.

No part of this publication may be reproduced and/or published by print, photoprint, microfilm or any other means without the previous written consent of TNO.

In case this report was drafted on instructions, the rights and obligations of contracting parties are subject to either the General Terms and Conditions for commissions to TNO, or the relevant agreement concluded between the contracting parties. Submitting the report for inspection to parties who have a direct interest is permitted.

© 2015 TNO

Summary

Foam Assisted Lift is a deliquification method to postpone liquid loading or to remove downhole accumulated liquids. This report describes the development of a model that predicts the pressure drop of gas/liquid/foam pipe-flows and thus can assist in the design of a FAL-system.

This model development is part of the JIP Experimental foam selection, which aims to improve the understanding of the performance of surfactants and how to select the optimum surfactant for a specific situation.

The model developed describes the velocity profile in the film, flowing along the wall. This velocity profile is computed using a momentum and mass balance over the film in combination with closures for the film quality, the film viscosity and the interfacial friction factor. In the current model, the film is treated as a homogeneous fluid and entrainment into the gas core is neglected.

The developed film flow model is able to predict the pressure drop and liquid holdup of the experimental data set with a accuracy of ~25% for air/water flows and ~40% for air/foam flows for concurrent gas/liquid/foam flow conditions (i.e. above the liquid loading point).

Contents

	Summary	2
1	Introduction.....	4
2	Literature review	5
2.1	Observations of foam dynamics and rheology	5
2.2	Foam modelling	7
2.3	Summary	8
3	Film flow model.....	9
3.1	Momentum balance	9
3.2	Mass balance.....	10
3.3	Closure relations.....	11
3.4	Correlation with other measurement techniques.....	19
3.5	Model predictions.....	26
4	Conclusions	30
5	Bibliography.....	31
6	Signature	34
	Appendices	
	A Symbol list	
	B Film flow	
	C Experimental data	
	D Rheology of foams	

1 Introduction

Liquid loading is a well-known problem that occurs when 'wet' gas wells approach their end-of-life. Due to depletion of the reservoir, its pressure drops and as a consequence the flow rates in the well drop as well. When only dry gas is present in the well the reduced flow rates have no further effect. However, when a liquid phase is present (either production fluids or condensed fluids) the reduced flow rates are not effective in transporting the liquids to topside and they will accumulate downhole (liquid loading). When a well is loaded, it may still produce at a low metastable rate, produce intermittently or may not produce at all. Foam Assisted Lift (FAL) is one of the possible methods to remove the downhole accumulated liquids (deliquification) and/or improve the production. In order to design a suitable FAL-system prediction of foam flow is a prerequisite.

From practice, [SPE132659] states that critical velocities (at which liquid loading occurs) can be reduced by 50-80% using surfactants. An average reduction of the critical velocity by the application of a surfactant is about 50% according to [IPTC11028]. This value is based on field experience and taken as a rule of thumb in their foamer applications.

This report describes the development of a model that predicts the pressure drop of gas/liquid/foam pipe flows and thus can assist in the design of a FAL-system. This model development is part of the JIP Experimental foam selection, which aims to improve the understanding of the performance of surfactants and how to select the optimum surfactant for a specific situation.

In Chapter 2 a literature review is presented. This literature review covers the research on foams applied for deliquification, ranging from experimental to modelling efforts and from small-scale foam-characterisation setups to large-scale flow loops. Chapter 3 describes the film flow model in detail and shows the prediction of the pressure drop for the available data sets. The aim of the model is to provide an estimate of the pressure drop for gas/liquid/foam pipe flows, when information on the surfactant performance under field conditions is available (i.e. via a small-scale test). Conclusions on the model performance are given in Chapter 4. The appendices provide detailed background information on the film flow model (Appendix B), the data sets used in developing the closure relations (Appendix C) and the rheology of foams (Appendix D).

2 Literature review

A literature search has been performed using a combination of the following keywords : “foam”, “foamer”, “surfactant”, “(pipe) flow”, “deliquification”. The search has been performed at the OnePetro site and with standard Internet Search Engines. As a result about 40+ relevant papers have been selected, covering small scale foam characterisation (e.g. blender, sparger, rheology) and large scale flow loop tests, from experimental and/or theoretical point of view.

The majority of selected papers describe foam behaviour through experimental observations. The theoretical background to foamers (i.e. “surfactant chemistry”) is typically given as an introductory Chapter in foam-experimental PhD theses (refs. 8, 39) or as a Short Course during gas well conferences (refs. 22, 41), since understanding of the foam chemistry is well established. Such descriptions focus on the force balance acting on individual lamellae between gas bubbles, orientation of surfactant molecules and qualitatively touch upon foam dynamics, i.e. film drainage and break-up.

Experimental studies can be split into 1) simple (often mobile) test devices for foamer selection for direct field application in gas well deliquification and 2) laboratory flow loops that evaluate fluid flow behaviour (gas-foam-liquid) under controlled conditions, mostly at room temperature and atmospheric conditions.

The first category concerns mostly blender and Bikerman column sparge tests, at atmospheric pressure and temperature (refs. 22, 50, 51). These testing methods give mixed successes to whether the tested-optimal foamer is also field-optimal, but are a very common quick-check before using a specific foamer for deliquification of a gas well.

More advanced experimental setups are generally flow loop systems with a vertical section with instrumentation (refs. 9, 26, 34 - 38, 55). Vertical lengths range from 4-42m (excluding the Bikerman sparging columns), with a typical diameter of 40-50mm. Operating pressures range from atmospheric (majority) to ~15 bar and temperatures ranging from room temperature (majority) to ~100-120 °C.

Numerous conference presentations and papers present showcases of successful application of foamers for deliquification of gas wells (ref. 24). None of these presentations/papers provide sufficient detail to be of direct use for quantitative prediction of liquid loading under surfactant injection at conditions other than mentioned in the presentations/papers.

2.1 Observations of foam dynamics and rheology

In recent years significant effort has been put into understanding the fundamental contribution of foam to lifting liquids from vertical gas wells, especially by Van Nimwegen (refs. 34 - 38). They report that most of the foam is transported along the wall of the pipe, see Figure 2.1 (right graph).

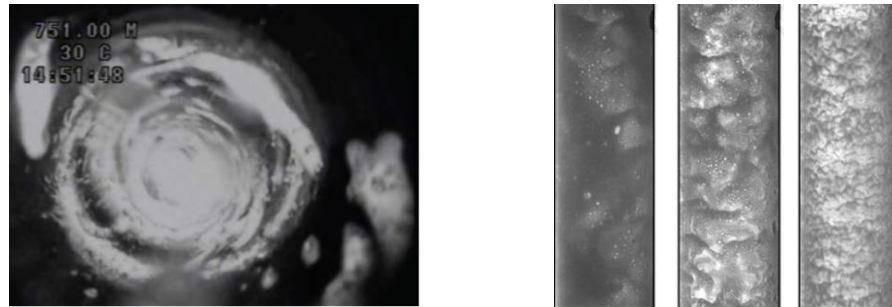


Figure 2.1. Left graph: snapshot of a movie showing a gas well that is being deliquified using surfactants (Miller 2009) taken from ref. 38. Right graph: snapshots of movies taken from the outside of a transparent pipe ($D = 50$ mm, $U_{sl} = 10$ mm/s, $C = 1000$ ppm Trifoam) showing gas/liquid/foam pipe flows with $U_{sg} = 6.4$ (Churn flow), 16.1 and 43 m/s (annular flow)(ref. 37). The critical velocity with 1000 ppm is about 5 m/s.

From the outside of a transparent pipe a gas/liquid/foam flow it also seems that wavy 'foam-structures' are transported along the wall for high U_{sg} (i.e. much larger than the critical gas velocity⁽¹⁾ at which liquid loading occurs), see Figure 2.1 (left graph). For flow velocities near but above the critical velocity, it is seen that foam waves move upward over a stagnant foam substrate.

As with all deliquification efforts, the effective shape of the TPC is key in predicting production time until loading. Figure 2.1 (right graph) shows the main observations from laboratory experiments: increased pressure drop at high gas flow rates and reduced pressure drop at low gas flow rates.

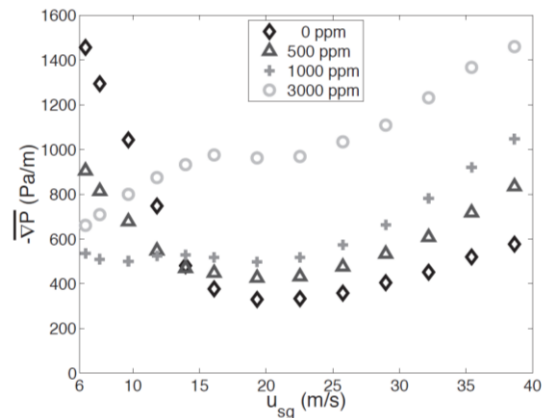


Figure 2.2. Right graph: tubing performance curve with various surfactant concentrations (ref. 39).

The significant shape change in TPC can be attributed to the shift of annular/churn flow to lower gas velocities (ref. 34). Observations vary among references, but the majority observes a shift to lower gas rates (or even absence) of churn flow (ref. 37 and references therein). Limited change of flow regimes was observed in (ref. 26). Foam changes the interfacial morphology and suppresses the formation and entrainment of large liquid droplets (or 'foam flakes') into the gas core. This affects the transition from annular to churn flow (shifted to lower gas rates by foam, ref. 38).

¹ The critical velocity at which liquid loading starts decreases with surfactant concentration.

The increased friction at high gas flow rates is attributed to a thicker foam layer at the tubing wall compared to the liquid film as it would be without foam (ref. 34). At the transition of annular/churn flow this foam film forms a static substrate, preventing immediate film flow reversal. The envelope of gas velocities at which this substrate forms varies for different surfactants (ref. 35).

The pressure drop below the TPC minimum can be reduced by 50% and is linked to a 50% reduction in liquid holdup (ref. 34). Pressure drop reductions up to 96% in slug flow were observed by ref. 26, attributing the pressure drop to a density drop by decreased bubble size as a result of surfactants. The largest reduction in gas flow rate at the TPC minimum is observed in ref. 35, shifting the critical rate from 21 to 1.6 m/s. Field observations however report typical reductions of a factor 2, ref. 7.

The observed foam stability is expected to increase interfacial shear by its increased viscosity (ref. 34) and is mentioned to be a function of 'blow ratio' (gas/liquid ratio), bubble diameter and concentration of a thickener (ref. 23). Variations of bubble size are in turn linked to foamer concentration, flow regime (ref. 35) and superficial liquid velocity (ref. 38).

Practical recommendations for rheology/viscosity measurements (and robust interpretation experimental data) are given in (ref. 20). These can be relevant especially when proceeding with experiments to better understand foam rheology as input for pressure drop modelling.

The observations from literature which are closest to being practical guidelines can be summarized as:

- With gas/liquid/foam flows liquid/foam is mainly transported along the pipe wall.
- Dynamic viscosity is a good measure for deliquification performance (ref. 51);
- The critical micelle concentration (CMC) is not a good predictor for required concentration to find a minimum pressure drop (ref. 35);
- The optimal foamer concentration increases with U_{sg} (gas flow rate) (ref. 35);
- Larger pipe diameters require larger surfactant concentrations for similar pressure drop (ref. 36).

2.2 Foam modelling

The three effects that surfactants have on a gas/liquid flow can be summarized as:

- Reduced static surface tension
- Reduced dynamic surface tension
- Formation of foam

Where especially the formation of foam leads to a significant reduction in pressure drop in vertical multiphase flow (ref. 37). Based on gas/liquid modelling of multiphase flow, various modelling approaches exist to predict the effect that foamers have on vertical gas flow.

In gas/liquid multiphase flow, the minimum pressure drop (TPC) is predicted by onset of either droplet or film flow reversal. Both can serve as a starting point for modelling the effect of foamers, as will be discussed below.

2.2.1 *Turner-based prediction of liquid loading*

In the prediction of liquid loading without surfactants, various modelling approaches are in use. The classic Turner model evaluates 'droplet reversal', i.e. the point at which flow drag no longer lifts a droplet upward. The Turner model (ref. 45) knows various modifications to account for e.g. large-wellbore application (ref. 46) and wellbore inclination (refs. 4, 52). Both the surface tension and liquid density are input parameters to the Turner-relation and therefore used to predict the effect of foamers (refs. 15, 25, 41, 50, 51).

2.2.2 *Film models*

The transition from annular to churn flow (near the TPC minimum) is in between the liquid loading and the flooding point. Flooding as a phenomenon can be split into three mechanisms, being 1) wave motion, 2) entrainment (droplet reversal) or 3) film flow reversal (ref. 33). Experimental observations at low pressure revealed that film flow reversal takes place at earlier stage than droplet flow reversal (ref. 49). Numerous authors have described the force balance over a film to estimate the pressure drop and the most critical flow regime transition: film flow reversal (onset churn flow) (refs. 2, 16, 19, 28, 29, 30, 33, 53, 54). None of the papers, however, discusses the effect of foam. Vice versa, none of the presented experimental foam studies makes the link to foam film modelling. This is however a logical next step based on observations of van Nimwegen (refs. 34 - 38) that churn flow is shifted to lower gas flow rates and predominantly foam film flow is present.

2.2.3 *Other models*

Soni made a first attempt to model the pressure drop of liquid-gas-foam flow using a drift flux model with a modified bubble velocity (ref. 44). This study is however questioned by (ref. 35), since it uses a different surface tension (of unrealistic value) for each of the analysed wells to obtain best results. No other mechanistic models were found in literature.

2.2.4 *Foam rheology*

Limited literature exists on practical modelling of rheology (viscous behaviour). It has been suggested to model foam as a pseudoplastic for pressure drop calculations, due to its shear-dependent viscosity (ref. 23). Examples of wall slip velocity are given in (ref. 20) and a critical view to the existence of yield stress in foam rheology is discussed. It furthermore stresses the importance of compressibility and in general gives practical recommendations for experimentally characterizing foam rheology (ref. 20).

2.3 **Summary**

The knowledge that foams are created by flow mixing or agitation has led to widespread use of open blenders or column spargers as initial foam performance evaluation tools. It is unknown if such experiments are representable to downhole conditions and the success rate of prediction is moderate.

Detailed observations of foam flow in experimental flow loops has provided insight to the effective dynamic behaviour of foam flow in gas wells. Furthermore, it gives a likely explanation to the fundamental change in effective tubing performance curve: the reduced presence of churn flow and increasing importance of foam film dynamics.

3 Film flow model

Based on the literature survey, a film flow model has been selected to predict foam flow behaviour. This film flow model has been developed using the available flow data on foam flows by : 1) TUDelft (van Nimwegen (ref. 39) and 2) TNO (Appendix C.1, C.2, C.14-C.17). These flow data consist of measured values of the pressure gradient, ∇p_z , the total film holdup before foam collapse, α_f , and the total liquid holdup after foam collapse, α_l . The flow data of TULSA University has not been used at present, since their data was lacking information on α_f .

The film flow model assumes that all liquid flows as a thin (aerated) film along the wall. The film thickness is constant along the pipe circumference and the interaction of waves with the gas core is only represented via an interfacial shear stress. There is no liquid transport by (individual) waves (waves are essentially averaged out). Liquid entrainment in the gas core is neglected⁽²⁾. The film flow model uses momentum and mass balances to estimate the film holdup that corresponds to a given flow condition specified by : the superficial gas and liquid velocity: U_{sg} and U_{sl} , the pipe diameter: D , and the surfactant concentration: C .

3.1 Momentum balance

A steady-state momentum balance in cylindrical coordinates is setup for the film at the wall (see Figure 3.1):

$$\frac{1}{r} \frac{\partial}{\partial r} r \tau = -\nabla_z p - (\rho_g \Gamma_f + \rho_l (1 - \Gamma_f)) g \quad (3.1)$$

where r is the radial coordinate, τ is the local shear stress, Γ_f is the local film quality (i.e. partial volume of free gas in the film), ρ_g and ρ_l are the gas and liquid phase density, g is the gravitational acceleration and $\nabla_z p$ is the pressure gradient. The term in brackets equals the film density, ρ_f ⁽³⁾.

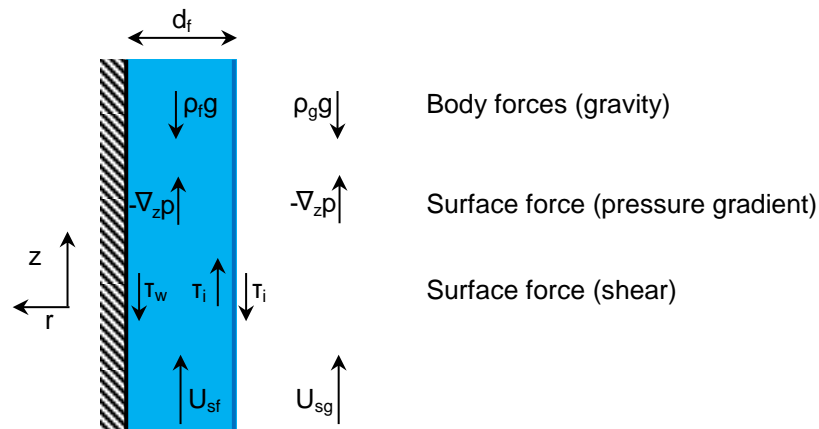


Figure 3.1 Sketch of film flow along the pipe wall showing forces acting on the film.

² Nimwegen (ref. 39) mentions that foamers suppress liquid entrainment significantly.

³ Here we have neglected that the gas density in the bubbles may be higher due to surface tension effects.

For a given interfacial shear stress, τ_i , pipe diameter, D , and film thickness, d_f , eq. 3.1 provides the shear stress profile in the film. Note that Γ_f is not necessarily spatially constant, but can be a function of local properties ⁽⁴⁾. Eq. 3.1 is integrated numerically to easily allow for a variation in local film quality.

It can be shown that a re-distribution of the mass within the film does not affect the value of the wall shear stress (i.e. as long as the mean film density, film thickness and interfacial shear stress remain constant, the wall shear stress is constant as well). Thus this distribution of mass does not directly affect the onset of negative wall shear (or the onset of liquid loading, see also footnote 4).

3.2 Mass balance

Using the shear stress profile obtained by eq. 3.1, the velocity gradient in the film, du/dy is calculated via:

$$\tau = -\mu_{f,tot} \frac{d}{dr} u \quad (3.2)$$

where $\mu_{f,tot}$ is the local viscosity of the film ⁽⁵⁾. Eq. 3.2 provides the velocity profile in the film (no-slip at the wall is assumed: $u_{r=\frac{1}{2}D} = 0$, see also Appendix B).

$$u = - \int_{D/2}^{D_c/2} \frac{\tau}{\mu_{f,tot}} dr \quad (3.3)$$

A negative film velocity near the wall marks the onset of liquid loading ⁽⁶⁾. The superficial liquid velocity is obtained via integration of the velocity profile taking into account the local film quality :

$$U_{sl,model} = \frac{4}{\pi D^2} \int_{D_c/2}^{D/2} (1 - \Gamma_f) u S dr \quad (3.4)$$

where $S = 2\pi r$ is the circumference of a circle with radius r ⁽⁷⁾. Using eqs. 3.1 and 3.4 with the relevant closure relations (see next section), the film model predicts $U_{sl,model}$ and $\nabla p_{z,model}$ depending on the film thickness, d_f :

$$d_f = \frac{1}{2}D(1 - \sqrt{1 - \alpha_f}) \quad (3.5)$$

where α_f is the total film holdup before foam collapse (i.e. including liquid and foam).

Figure 3.2 shows how the solver finds the solution for a flow condition (experiment #15.04). First $U_{sl,model}$ and $\nabla p_{z,model}$ are computed for a range of α_f . Then, the solver finds the best solution of α_f such that $U_{sl,model} = U_{sl,exp}$. This solution of α_f then also provides the solution for ∇p_z .

⁴ In this way the film can be described as, e.g., a lubricating liquid film at the wall with a foam layer flowing on top.

⁵ The local viscosity of the film can depend on, e.g., the local shear stress value (non-Newtonian behavior) as well as local turbulence intensity (apparent viscosity).

⁶ With the no-slip condition at the wall a negative film velocity near the wall is similar to a negative wall shear.

⁷ Eq. 3.4 is the film flow solution with circulation (see appendix B.6).

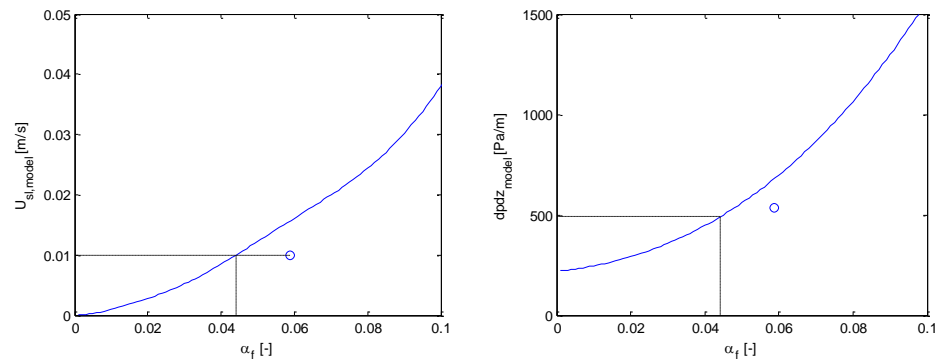


Figure 3.2 Calculated superficial liquid velocity (left graph) and pressure gradient (right graph) as a function of film holdup. The symbols represent the measurement data corresponding to experiment #15.04. The dashed black line indicate the solution found by the film holdup solver.

3.3 Closure relations

In order to solve the momentum and mass balance for the film, closure relations are required to have a closed system of equations. The closure relations that are needed are for :

- the film quality, Γ_f ,
- the film viscosity, μ_f , and
- the interfacial friction factor, f_i .

Closure relations should be designed to capture the physics best. Therefore, each section on the closure relations starts with a description of the relevant physics, if possible, aiming to provide an explanation for the chosen dependencies.

3.3.1 Film quality

For air/water flows there is no closure relation required for the quality of the film. The quality of the film is zero (i.e. pure liquid). Any entrainment of gas into the liquid film is neglected ⁽⁸⁾.

With air/foam flows, foam is created by entrainment of gas into the liquid film, which increases the quality of the film. The mean film quality of the experiments with air-foam flows is calculated via :

$$\langle \Gamma_f \rangle = 1 - \frac{\alpha_l}{\alpha_f} \quad (3.6)$$

where α_f is the total film holdup before foam collapse, and α_l is the total liquid holdup after foam collapse (see section C.1 on a detailed description of the measurements of α_f and α_l).

⁸ Note that with churn flow conditions (aerated irregular slugs) this may be less accurate.

Gas entrainment is expected to be caused by wave overtopping. Large waves may be more efficient in entraining gas into the liquid film due to their size. Since the size of the wave structures usually are related to the film thickness, an increase of the mean film quality with film thickness is thus expected. This is also observed in Figure 3.3.

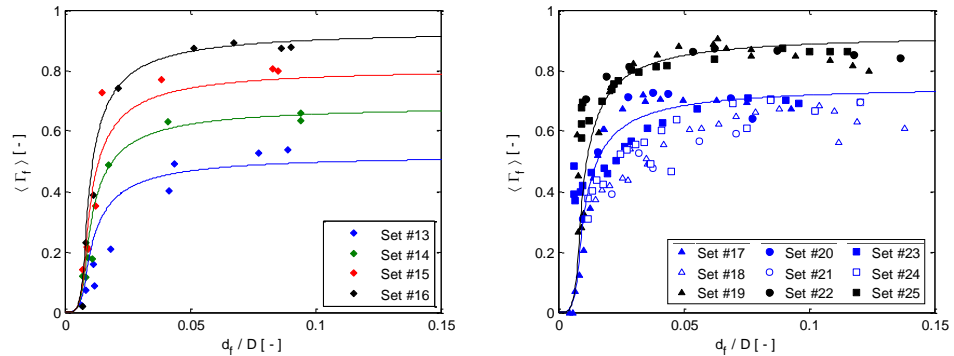


Figure 3.3 Mean film quality (eq. 3.6) versus the normalised film thickness (eq. 3.5) for the Foamatron data sets (left graph, datasets #13 to #16) and Trifoam data sets (right graph, datasets #17 to #25). The solid lines represent eq. 3.7 for the various surfactant types and concentrations. For the higher values of d_f/D (i.e. $> \sim 0.1$), the flow pattern tends to be churn flow (see Figure 2.1, right graph with $U_{sg} = 6.4$ m/s).

Besides the entrainment of gas into the film, also the residence time of the gas bubbles in the liquid film is important. Increasing the bubble residence time (i.e. increasing foam stability) results in an increase in gas accumulation, hence increase in mean film quality. Since an increase in surfactant concentration gives a more stable foam, the mean film quality is expected to increase with increasing surfactant concentration. This is also observed in Figure 3.3.

From Figure 3.3 it also seems that for a film thickness below a critical value, $d_{f,crit}$, the mean film quality is zero (i.e. base liquid). This may be attributed that for a very small film thickness overtopping waves hardly exist⁽⁹⁾, which prevents the creation of foam.

Finally, Figure 3.3 also indicates an asymptotic behavior for larger film thicknesses, depending on the surfactant concentration. The following may be responsible for this behavior :

- In this range of film thicknesses ($d_f/D > \sim 0.1$), the flow pattern is a churn flow, which is more alike highly aerated irregular slugs than a wavy film. The correlation between d_f and Γ_f as found for annular flows, may not hold anymore⁽¹⁰⁾.
- With increasing foam quality the total amount of free-surface area increases. Hence also the total amount of surfactant molecules required. Possibly, the

⁹ For gas/liquid systems it is also observed that a minimum holdup is required to create droplets (which emerge from the crests of waves). In most cases this is reflected in a minimum film Reynolds number: Re_{film} .

¹⁰ It seems that in churn flow an increase in holdup does not result in a more efficient mixing of gas into the film and/or decreases the foam stability. This may be due to an increase in pressure fluctuations or shear and/or a change in the timescales for surface renewal.

horizontal asymptote (or maximum achievable quality) is related to the limited surfactant concentration.

An attempt to capture the above features in a closure relation for the mean film quality is made using :

$$\langle \Gamma_f \rangle = \begin{cases} 0 & d_f \leq d_{f,crit} \\ A_\Gamma \left[1 - \frac{d_{f,crit} - d_{f,0}}{d_f - d_{f,0}} \right] & d_f > d_{f,crit} \end{cases} \quad (3.7)$$

Where A_Γ represents the horizontal asymptote and $d_{f,0}$ the vertical asymptote.

The values for the various parameters that represents the data overall best are :

$$d_{f,crit} = 6 \cdot 10^{-3} D \quad (3.8)$$

$$d_{f,0} = 3.6 \cdot 10^{-3} A_\Gamma D \quad (3.9)$$

Eq. 3.7 is presented in Figure 3.3 (solid lines) together with the experimental data of the Foamatron and Trifoam data sets.

The parameter A_Γ depends on the surfactant type and concentration and is shown in Figure 3.4 (left graph). It is noted that the dotted lines in Figure 3.4 are only intended to connect the A_Γ -values of the two surfactants, and should not be used for extrapolation beyond the maximum surfactant concentration used for a given surfactant. Actually, the functions used to connect the A_Γ -values of the two surfactants allow for A_Γ to exceed one, which is not physical.

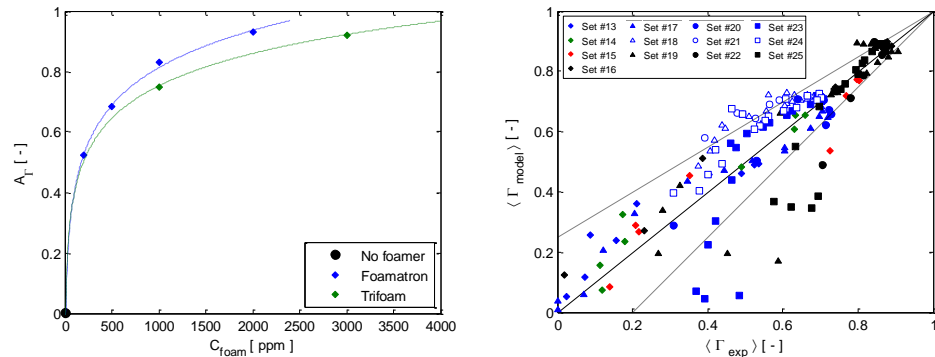


Figure 3.4 Left : horizontal asymptote for the film quality, A_Γ , as a function of the concentration for Foamatron (blue) and Trifoam (green). For a foamer concentration of zero, the value of A_Γ equals zero. The dotted lines connect the values of A_Γ . Right: prediction of the film quality using eq. 3.7 and the 25% error lines (dashed curves) for $(1 - \langle \Gamma_f \rangle)$.

The predicted values of the mean film quality using eq. 3.7 are plotted against the experimental data in the right graph of Figure 3.4. The dotted lines represent the 25% error lines for $(1 - \langle \Gamma_f \rangle)$, which is used in eqs. 3.1 and 3.4. Data sets #23 to #25 (i.e. $D = 80$ mm) show largest deviation from eq. 3.7, which is tuned to fit data sets #17 to #25 overall best.

In section 3.1 it is mentioned that the local film quality is not necessarily constant. The developed film flow model is capable of dealing with a spatial distribution of the liquid within the film (e.g. having a liquid lubrication layer at the wall with a foam layer flowing on top). However, the experimental data available is too limited to substantiate a spatial variation of the local film quality.

3.3.2 *Film viscosity*

In the model, the film viscosity is the sum of the bulk viscosity of the fluid flowing along the wall and the apparent turbulent viscosity.

3.3.2.1 *Turbulence viscosity*

For the apparent turbulent viscosity of the film, μ_τ , as a function of the distance to the wall, $y = \frac{1}{2}D - r$, the mixing length theory with Van Driest wall damping is used :

$$\mu_\tau = \rho_f \ell_m u_\tau = \rho_f \kappa y u_\tau [1 - \exp(-y/d_\mu A^+)] \quad (3.10)$$

$$d_\mu = \mu_f / \rho_f u_\tau \quad (3.11)$$

$$\rho_f u_\tau^2 = \tau_c = \frac{1}{3}(2\tau_w + \tau_i) \quad (3.12)$$

Where ℓ_m is the mixing length, u_τ is the friction velocity, κ is the von Karman constant (= 0.41), d_μ is the viscous length scale, A^+ is the van Driest constant and τ_c is a characteristic shear stress.

For single phase boundary layers A^+ typically has a value of 26, however, in annular flows the turbulence intensity of the film seems less strong. This is also reported by Ashwood et al. (2015, ref. 3). They measured the velocity profile in the liquid film of an annular flow using PIV. The above model for the apparent turbulent viscosity has been fitted to their data and results in a best fit for $A^+ = 150$ (see Appendix B.7).

3.3.2.2 *Foam viscosity*

The viscosity of foam depends strongly on the water content, see section 3.4.2. For a high quality foam (i.e. dry foams : $\Gamma > \sim 0.9$), foam can be described as a shear-thinning fluid with a yield-stress (e.g. ref. 48). However, when the quality is low (i.e. $\Gamma < \sim 0.6$), foam is better characterized as a bubbly liquid and can show Newtonian behavior. For intermediate quality, foam shows a shear dependent viscosity, but without yield-stress (see also section 3.4.2).

A film viscosity μ_f is computed such that the experimental air/foam flow data fits the film flow model via the following steps :

- The measured pressure gradient and total film holdup are used to compute the shear stress profile in the film via eqs. 3.1 and 3.5.
- From this shear stress profile the velocity gradient is computed using a viscosity, μ , and taking into account turbulence effects (with $A^+ = 150$).
- This velocity gradient is integrated twice to obtain the liquid superficial velocity (eqs. 3.2 to 3.4), whereby the film quality is determined by eq. 3.6 (i.e. the measured mean film quality is used).
- Obviously, the calculated liquid mass flow depends on the chosen value for μ : increasing μ will decrease the velocity gradients, hence also the liquid mass flow. The film viscosity, μ_f , is defined as the value of μ for which the calculated liquid mass flow equals the liquid mass flow of the flow condition.

In Figure 3.5, the computed film viscosity is shown for all experimental conditions with air/foam flows with positive wall shear (i.e. for which liquid loading is not yet occurring).

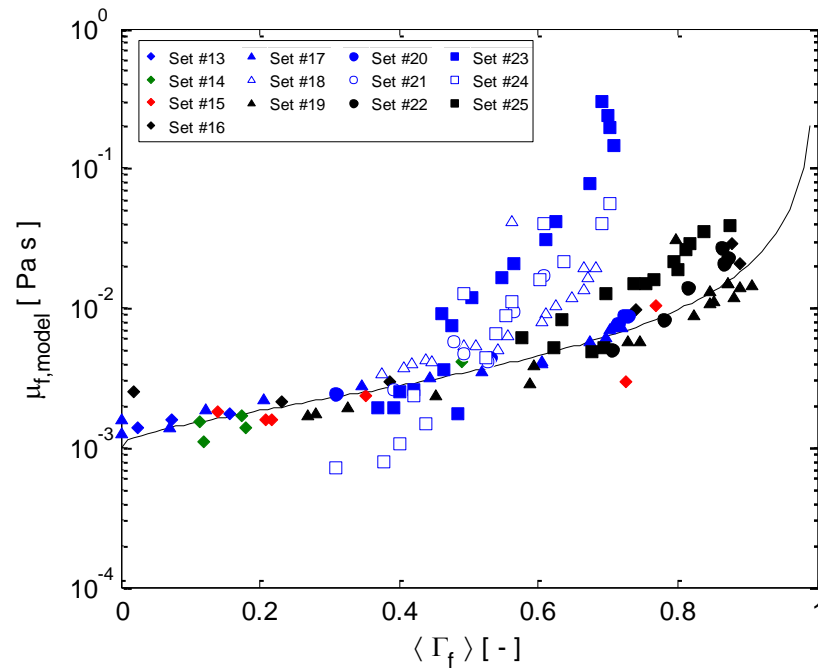


Figure 3.5 Computed film viscosity for all air/foam data sets. The solid line represents the foam model of Mitchell (1960).

To predict the film viscosity, the model of Mitchell (1960, ref. 32) is used :

$$\mu_f = \frac{\mu_l}{1 - \Gamma_f^n} \quad (3.13)$$

This model is developed by Hatchek (1911), who used $n = 0.33$. Mitchell (1960, ref. 32) modified this value to $n = 0.49$, which better represented his experimental foam viscosity data. In the remainder of the report the model of Hatchek-Mitchell (i.e. $n = 0.49$) is used to estimate the local film viscosity.

The computed film viscosity values are scattered significantly around the model prediction of Mitchell. Especially, for the data sets with the 80 mm flow loop the computed viscosity is not captured well by eq. 3.13. Possibly, for these data sets the film viscosity is closer to bulk foam viscosity than for the data sets with $D = 34$ mm or $D = 50$ mm, because the d_f is larger (see also section 3.4.2). The values of μ_f that lie significantly below the line as predicted by Hatchek-Mitchell is likely to be caused due to a too small value of A^+ (i.e. the turbulence intensity in the film is overestimated using $A^+ = 150$). However, the data currently available does not allow for A^+ be depending on the presence of foam.

3.3.3 Interfacial friction

The experimental interfacial friction factor, $f_{i,exp}$, is calculated for all data sets using:

$$\tau_i = \left(\frac{dp}{dz} - \rho_g g \right) \frac{D-2d_f}{4} = f_{i,exp} \frac{1}{2} \rho_g U_{sg}^2 \left(\frac{D}{D-2d_f} \right)^4 \quad (3.14)$$

Pressure drop effects due to entrainment of droplets into the core are implicitly taken into account in $f_{i,exp}$.

3.3.3.1 Air/water flows

Figure 3.6 shows the experimental interfacial friction factor, $f_{i,exp}$, for all air/water data sets as a function of Re_{sg} and d_f/D .

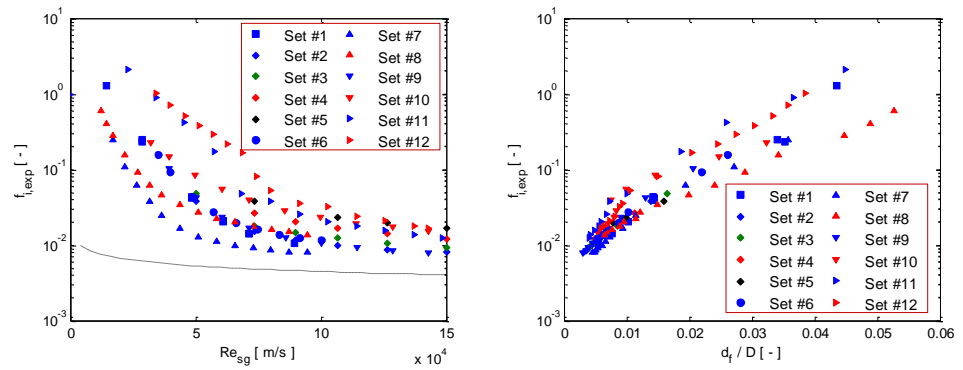


Figure 3.6 Experimental interfacial friction factor versus Re_{sg} (left graph) and d_f/D (right graph) for all air-water data sets (set #1 to #12). For comparison, the smooth wall Blasius friction factor is shown as well (left graph, dashed line).

A closure for the interfacial friction factor has been developed to capture the trends of the air/water data best :

$$f_i = f_G \left(1.5 + 100 \frac{d_f}{D} + \gamma \frac{d_f^2}{D^2} \right) \quad (3.15)$$

$$f_G = 0.0791 Re_{sg}^{-0.25} \quad (3.16)$$

$$\gamma = A_\gamma D^2 + B_\gamma D + C_\gamma \quad (3.17)$$

With $A_\gamma = 1.5 \cdot 10^7 \text{ m}^{-2}$, $B_\gamma = -6.7 \cdot 10^5 \text{ m}^{-1}$, $C_\gamma = 2.0 \cdot 10^4$.

The right graph of Figure 3.7 shows $f_{i,exp}$ normalized using this closure. For comparison, the left graph of Figure 3.7 shows $f_{i,exp}$ normalized using the correlation as given by Fore et al. (2000, ref. 16), which indicates the improvement of the interfacial friction factor closure for the air/water data sets.

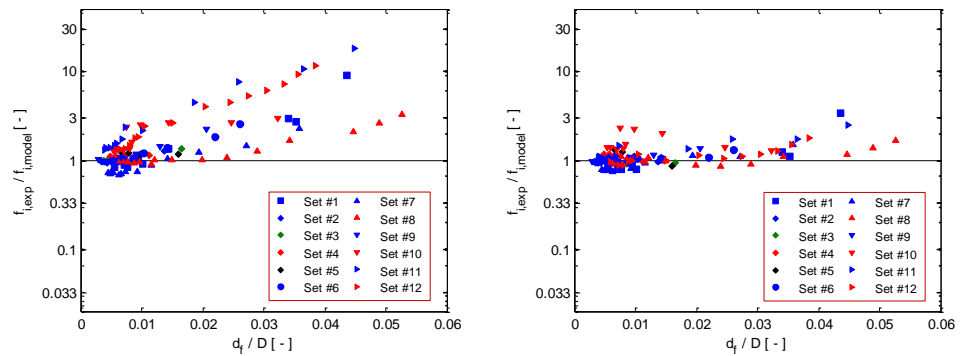


Figure 3.7 Left: $f_{i,exp}$ normalised using the correlation of Fore et al (2000, ref. 16). Right: $f_{i,exp}$ normalised using eqs. 3.15 and 3.16.

3.3.3.2 Air/foam flows

The experimental interfacial friction factor for all air/foam data sets is shown in Figure 3.8.

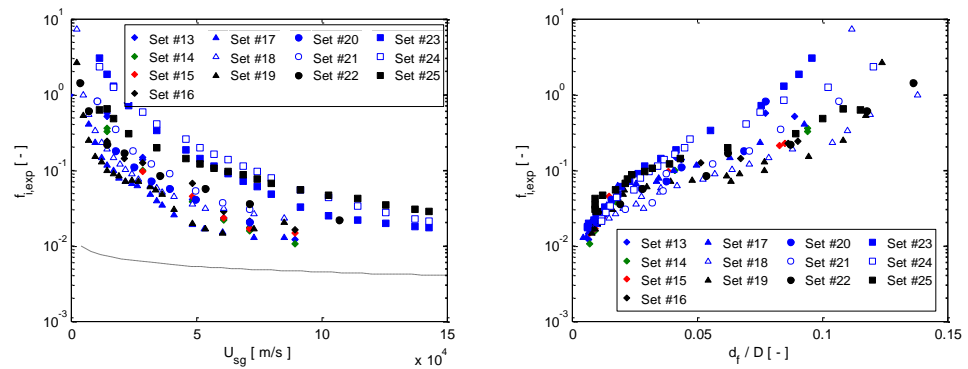


Figure 3.8 Experimental interfacial friction factor versus U_{sg} (left graph) and d_i/D (right graph) for all air-foam data sets (set #13 to #25). For comparison, the smooth wall Blasius friction factor is shown as well (left graph, dashed line).

For high $U_{sg}^{(1)}$, the interfacial friction factor increases with increasing surfactant concentration. This may be caused by the reduction of the surface tension of the base fluid, which leads to a decrease in surface curvature (i.e. an increase in surface roughness).

For low U_{sg} , it is observed that the interfacial friction factor decreases with increasing surfactant concentration. Possible reasons for this effect may be :

- Damping of waves by the increased viscosity of the foam.
- Suppression of wave crests : (foam bubbles may smooth the waviness of the film)

¹¹ For these conditions there exists little foam (i.e. $\Gamma_1 \sim 0.4$).

Eq. 3.14 has been modified to include these effects :

$$f_i = f_G \left(\beta + 100 \frac{d_f}{D} + \gamma \frac{d_f^2}{D^2} \right) (1 - \langle \Gamma_f \rangle) \quad (3.18)$$

$$\beta = 1 + A_\beta \sqrt{\max(C, C_{\min})} \quad (3.19)$$

with, for Foamatron : $A_\beta = 0.09 \text{ ppm}^{-0.5}$ and $C_{\min} = 30 \text{ ppm}$, and for Trifoam : $A_\beta = 0.06 \text{ ppm}^{-0.5}$ and $C_{\min} = 70 \text{ ppm}$. C_{\min} is chosen such that eqs. 3.18 and 3.19 converge to eq. 3.14 for small foamer concentration.

Figure 3.9 shows $f_{i,\text{exp}}$ for all air/foam flows normalised using eqs. 3.18 and 3.19.

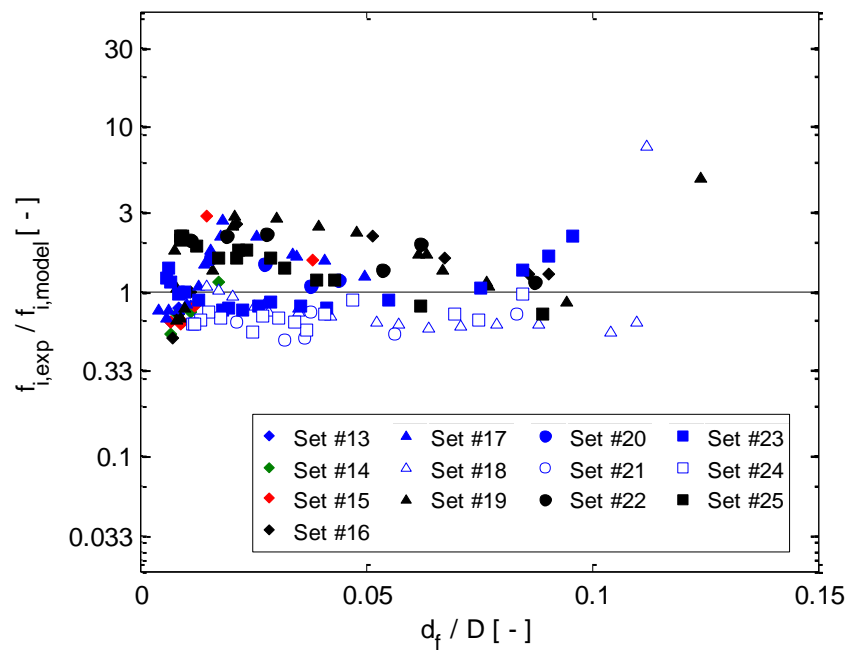


Figure 3.9 Measured interfacial friction factor normalised with eqs. 3.18 and 3.19 versus the measured normalised film thickness for all air-foam data sets.

3.4 Correlation with other measurement techniques

3.4.1 Film quality

In section 3.3.1, the film quality $\langle \Gamma_f \rangle$ has been correlated to the mean film thickness, d_f , to describe the foaming at the interface due to the wave action. In this correlation A_Γ is the key parameter that describes the surfactant behaviour and it depends on surfactant type and concentration. A high value of A_Γ leads to low values for $\langle \Gamma_f \rangle$ when d_f is sufficiently large. Thus, A_Γ describes the improvement of mixing gas and liquids by the addition of surfactants. This mixing, in turn, is related to the foamability of the surfactant solution.

Foamability is defined in WP4 as the ability 1) to create foam (build-up test) and 2) to unload liquid (carry-over test). Thus, a comparison between A_Γ and the tests of the small scale setup (build-up and carry-over) has been made to judge if A_Γ can be predicted using only small scale tests results. The benefits for this method are that large scale flow tests (costly and time consuming) could be avoided, which is especially preferred in case tests are required with field fluids and/or at field conditions (elevated pressure/temperature).

The carry-over tests of the small scale setup are chosen to be correlated to A_Γ , since they show better reproducibility than the build-up tests and are more directly related to the process of deliquification. In Figure 3.10 A_Γ is plotted against the relative total carry-over⁽¹²⁾ at identical conditions (surfactant type and concentration); the results for three sparger gas flow rates are presented.

From Figure 3.10 it is observed that increasing the carry-over the value of A_Γ will increase, which increases $\langle \Gamma_f \rangle$ at low gas velocities and improves the liquid unloading by lowering the hydrostatic pressure. Therefore, a correlation between the small scale carry-over and A_Γ seems suitable, even though the processes of foam creation are different in both systems⁽¹³⁾.

For the lowest sparger gas flow rate ($U_{sg} = 0.01$ m/s), the carry-over in the small scale is reported to be influenced strongly by drainage, which is expected to be of negligible importance in the flow loop tests. The intermediate and high sparger gas flow rates are correlated to A_Γ via :

$$A_\Gamma = 0.4 + 0.6 CO_{tot} \quad (3.20)$$

where CO_{tot} is the relative total carry-over at intermediate / high sparger gas flow rates.

Eq. 3.20 is not expected to be accurate for near-zero carry-over values (i.e. relatively low surfactant concentrations), but under these conditions the surfactant is not expected to have a significant effect anyways.

¹² The relative total carry over is the total amount of liquid carried over to the carry-over vessel normalised by the amount of liquid initially presence in the bubble column. The total carry-over may be affected by surfactant depletion at the end of the test, but is more robust in terms of post-processing than the linear carry-over.

¹³ Note that ref. 44 also relates the film quality to the carry-over.

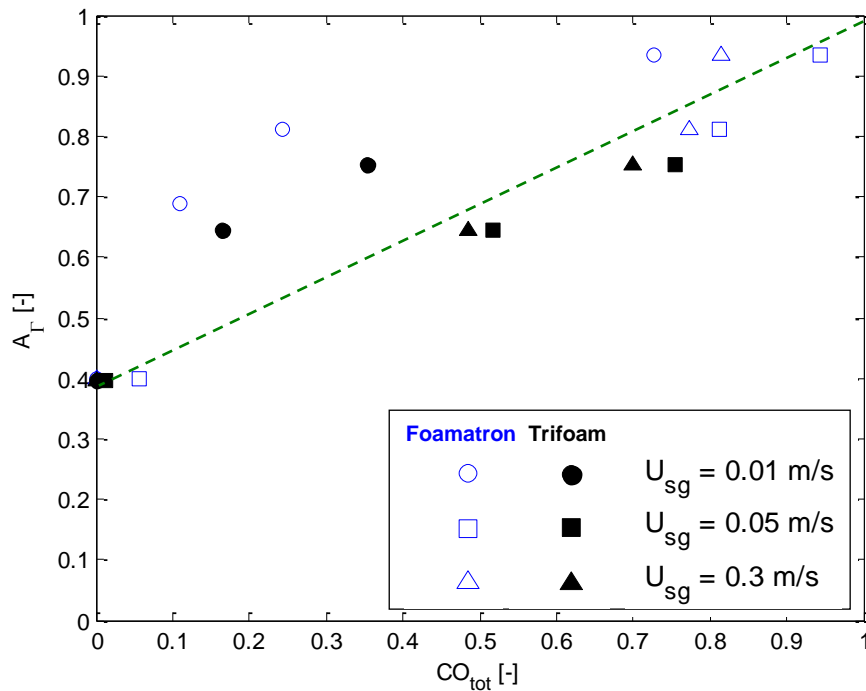


Figure 3.10 A_r as a function of relative total carry-over at similar conditions (surfactant type and concentration) for three different sparger gas flow rates. The dashed green line is a first model attempt (eq. 3.20).

3.4.2 Foam viscosity-rheology

There are two reasons to study the rheology of foams.

- Find out if the film model predictions are best by using the viscosity closure model of Mitchell (eq. 3.13) or by determining experimentally the relation between viscosity and foam quality.
- Investigate the possibility to retrieve properties from rheological measurements that can be related to the performance of the surfactants in practice.

The model of Mitchell is a relative straightforward relationship between the viscosity and the foam quality. There are a number of aspects that are not taken into account. For one the relationship is for a water-air surfactant system in the absence of e.g. any condensate or salt. Also there is no dependence on the type of surfactant nor on shear rate. Maybe therefore the model does not reflect the viscosity in practice. Here the viscosity data determined experimentally is compared with the model of Mitchell.

Also a comparison is made between the directly measured viscosity values and the values of the viscosity that can be calculated on the bases on the experimental data from the flow experiments as given in Figure 3.5.

In the rheology experiments the viscosity is determined in a configuration of concentric cylinders and continuous rotation as this configuration reflects best the conditions in liquid loading.

The viscosity is related to the friction force needed to generate a given laminar flow. For homogeneous Newtonian materials this relation is straightforward and does not depend of flow conditions. For complex materials like foams the relationship between the force needed for a given flow however is quite complex and depends on many parameters. From measurements where an oscillatory movement is imposed and the resulting oscillatory force needs to be exerted, it is possible to retrieve information about the structure of the foam without disturbing the structure. Also information under what deformations and forces the structure starts to fail. These last properties are related to the strength of the foam lamella and therefore the mechanical stability of the foam. The 'oscillatory experiments' are not directly related to the present modelling and are therefore elaborated in Appendix D together with the theoretical background of rheological measurements.

3.4.2.1 *Experimental determination of viscosities*

In the model of Mitchel it is implicitly assumed that the foam is a homogeneous material with a given set of properties. Therefore the rheology of the foam as it is present in the liquid film is studied; note that the experimental setup determines the 'bulk properties' of the foam.

The directly measured viscosities are determined by concentric 'cylinders'. An experimental set-up was developed to allow the measurement of the bulk rheological properties of the foam under controlled conditions (i.e. foam quality, shear stress, strain rate),

As foams age in time it is important to perform the measurements on freshly formed foam. To that end a gas flow and a liquid flow are combined and pumped from the bottom through a glass filter that serves as a sparger. The cup of the glass filter serves as the outer cylinder in the measurement. In this way at all times fresh foam is in the measuring cylinder.

Slip at the wall of the inner cylinder (rotor) can be an important source of an experimental error as there is always a small layer of liquid present between the foam and the wall. This leads to slip near the wall and therefore causes an underestimation of the viscosity of the foam. Therefore, an axis with 4 blades is used as a rotor instead of the standard solid cylinder. The foam is trapped between the blades and therefore more or less behaves like a solid cylinder of foam.

The viscosity is measured by recording the torque of the rotor needed to rotate the rotor with a given speed.

The distance between the wall of the cup and the outer edge of the blades of the rotor is large enough to accommodate a number of bubbles. In this way the viscosity is representative for the bulk viscosity.

The quality of the foam is varied by the adaptation of the ratio of the nitrogen and liquid flows.

The slip at the outer wall of the cup was neglected as it was expected to play a minor role.

Figure 3.11 shows a picture of the set-up. For more details on the developed setup, see Appendix D.

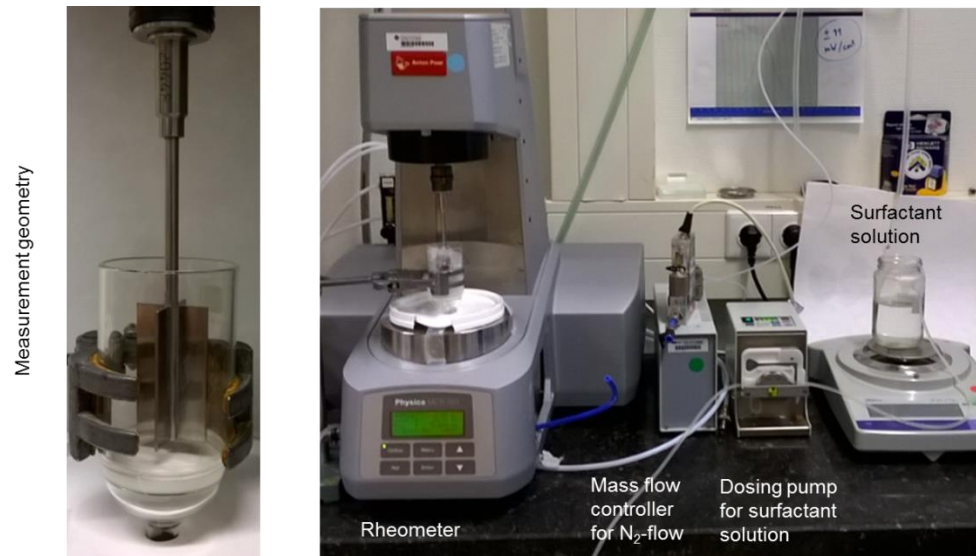


Figure 3.11 The set-up is fitted into an Anton Paar rheometer. Left detail of measuring geometry of rotor with blades in glass filter.

3.4.2.2 *Experimental results*

For different foam qualities the viscosity was measured as a function of the shear rate. The data are given in Figure 3.12. A number of clear trends are found. At high foam qualities the foams show a shear thinning behaviour. However, at low foam quality the viscosity show little dependence on shear rate and can be considered to be Newtonian-like. The difference in behaviour is due to the fact that at high qualities the foam is a traditional foam with a lot of thin lamellae. In contrast, for the foams with low quality the bubbles hardly touch each other and can be considered as bubbly liquids.

Further it is quite remarkable that the curves of logarithm of the viscosity as a function of the shear rate is close to a linear relationship. The upturn of the curves at the high shear rate range is due to turbulence. It can be seen that the onset of the range where the foam shows turbulence is higher for foam with higher quality. This may be attributed to the higher viscosity or the structure in the foam preventing turbulent currents.

3.4.2.3 *Comparison of measured data and model of Mitchell*

Figure 3.13 shows two curves that represent the theoretical values as calculated by means of the model of Mitchell with two different exponents that are reported in literature. Also three experimental curves are given at different shear rates. The shear rate in the flow experiments is estimated to be around 900 s^{-1} on average. The curves at shear rates of 1 s^{-1} and 10 s^{-1} are the actually measured data points. The values at shear rate of 100 s^{-1} are extrapolated values as under these conditions turbulence effects become noticeable.

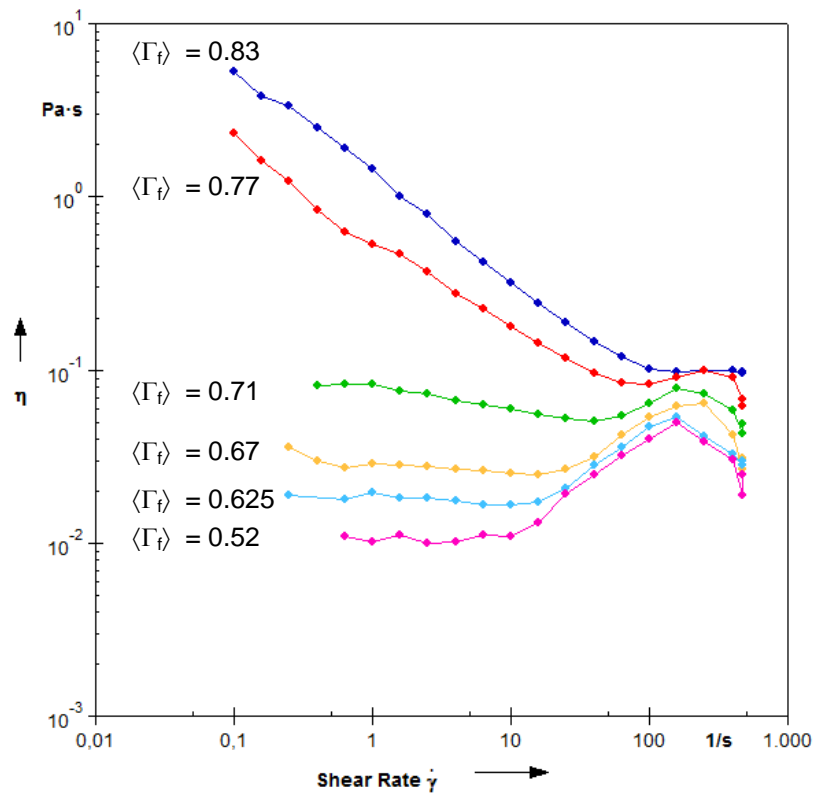


Figure 3.12 Viscosity as a function of shear rate with various foam quality.

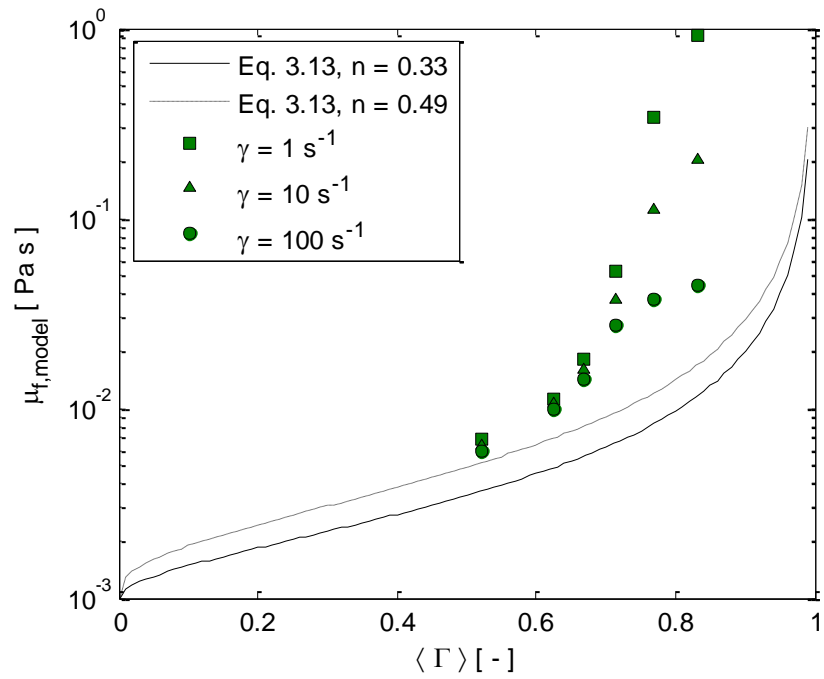


Figure 3.13 Viscosity as a function of wetness for various shear rates.

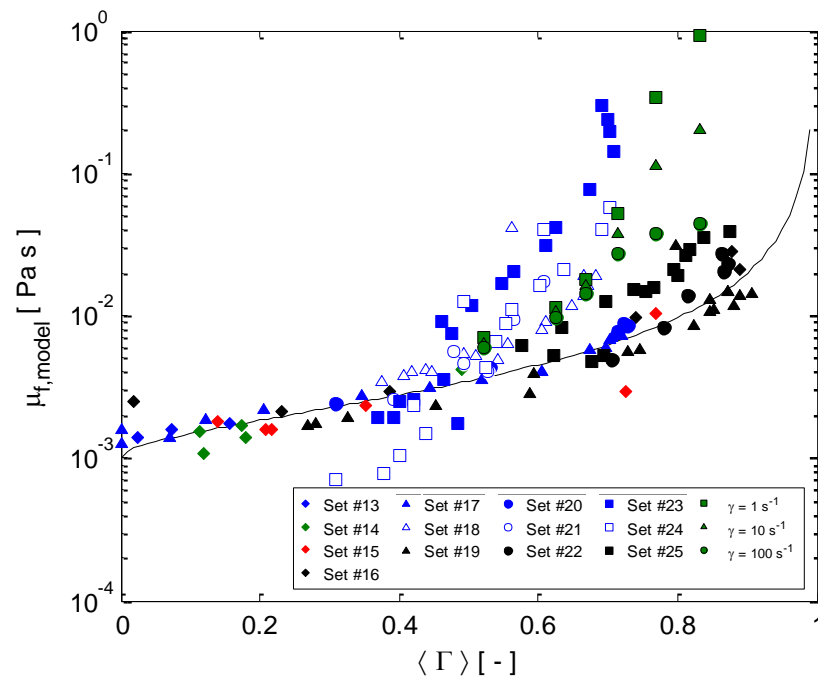


Figure 3.14 Measured viscosities (with various shear rate), computed film viscosity (from Figure 3.5) and the foam viscosity model of Mitchell (solid line).

From Figure 3.13 it is clear that the experimental data cannot be fitted to the values of the model of Mitchell. Slope of the curves of the logarithm of viscosity as function of foam quality is higher for the experimental data than predicted by the model of Mitchell. Adaptation of the exponent n in the equation leads to a vertical shift of the curve but does not tilt the curve. At higher shear rates the curves tend to have a lower slope, which comes closer to the slope encountered in the model. This is because the influence of shear rate is largest at high foam quality because dry foams with adjacent bubbles are more structured than wet foams and the disturbance of the structure under flow is larger than in wet foams.

Also it is observed that the experimental values show some kind of an s-curve with the highest slope in the middle range. From other data series with oscillatory measurements (see Appendix D) it shows that this would even be more pronounced if more values at higher quality would have been included as viscosity values level off in that range.

For the wet foams the measured values and the calculated values are closer together, as in that range the foam strongly resembles bubbly liquid and is more or less Newtonian.

Figure 3.14 shows the experimental data determined with the rheometer together with the viscosities calculated from the flow experiments (Figure 3.5). A first conclusion is that the measured viscosities are in the same range as the values calculated from the flow experiments. Closer inspection shows that at low shear rate the data are closer to the values obtained from the series executed with pipes of 80 mm diameter. However, at high shear rate the data come closer to the values of the series of 34 and 50 mm.

First it is checked if there was also a difference in shear rate between the sets of flow experiments. This seems to be the case. What is observed is that for all series

of flow experiments at high quality (corresponding to 'churn flow'), the shear rate is relatively low in the order of a few tens s^{-1} . This would mean conditions between the experimental values at shear rate of 10 s^{-1} and 100 s^{-1} . At low foam quality the shear rate is much higher (about 100 s^{-1} to 1000 s^{-1}).

Next the thickness of the foam layer in the tubing was checked. It appears that the film thickness for the series of experiments with the 80 mm diameter tubes are significantly higher (scales with pipe diameter). For the 80 mm series the thickness of the foam layer at high foam quality (low gas velocities) is in the order of 1 cm and decreases down to a few hundreds microns. For the 34 and 50 mm series the thickness starts at around 4-5 mm and again decreased to the sub-millimetre range. It may very well be that the higher thickness of the foam layer gives an apparent viscosity that is closer to bulk values and that thinner layers give apparent values that are more dictated by wall effects. Near the wall there is always a small liquid layer that has a much lower viscosity than the bulk values.

If we look at the conditions of the measurements of Mitchell it is noted that they determined the viscosities of foam by measuring the pressure drop between the beginning and end of the tubes with a small diameter. These tubes typically are very narrow. (0.029 – 0.092 inch) and flow experiments with foam are executed at high shear rates ($200 - 9000 \text{ s}^{-1}$). The small diameter makes that the wall effects cannot be neglected giving viscosity values that are lower than bulk foam values. So both high shear rate and wall effects make that his model probably predicts viscosities much lower than bulk values.

3.4.2.4 Conclusions

In the present modelling of the viscosity as used in the film model there are no effects included of shear rate and/or of the film thickness. The Mitchell model serves his cause as it allows a good prediction of the TPC for the present experiments.

On the other hand it is shown that there is a big influence of shear rate and there is a wide range of shear rates encountered for the different conditions. Also it seems that layer thickness may play an important role. We expect if we want to improve the prediction especially under real life conditions we will need to include these effects.

For the measured viscosities it was demonstrated that values that were determined are in the right range and trends of foam quality and shear effects can clearly be determined. If the hypothesis is right it means that for a better prediction wall effects need to be taken into account. Viscosity measurements with different gaps between inner and outer cylinder may be used to account for this effect.

These viscosity measurements also hold the promise that it is possible to study the effect of the presence of salts and hydrocarbons to mimic the effect of condensate (emulsions) and type of surfactant.

3.5 Model predictions

The film flow model eqs. 3.1 – 3.5 together with the closure relations for the film quality (eqs. 3.7 – 3.9), the film viscosity (eqs. 3.10 – 3.13) and the interfacial friction (eqs. 3.16 – 3.19) have been used to predict the flow at the conditions of all data sets. The results of the pressure gradient, film holdup and total liquid holdup are compared against the experiments in the following sections. The results are plotted against the densimetric gas Froude number, F_g , given as :

$$F_g = \frac{U_{sg} \sqrt{\rho_g}}{\sqrt{gD} \sqrt{\Delta\rho}} \quad (3.21)$$

Typically, the onset of LL is expected to be near $F_g = 1$ (especially for smaller pipe diameters: $D < \sim 100\text{mm}$).

Here the focus has been on the overall predictability of the available data sets and not on the predictability of the critical velocity and corresponding pressure gradient ⁽¹⁴⁾.

3.5.1 Air/water flows

In Figure 3.15 and Figure 3.16 are presented the experimental pressure gradient and film holdup normalised by the model predictions for all air/water flows, respectively.

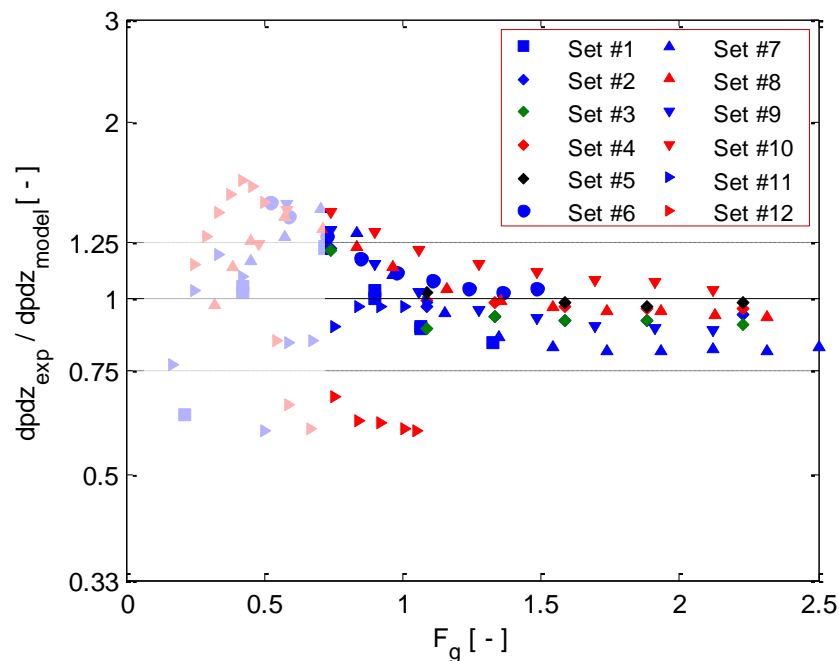


Figure 3.15 Experimental pressure gradient normalised with the model results for all air/water data sets. For $F_g < \sim 0.8$ flow reversal occurs, where churn flow is expected to exist (blanked data).

¹⁴ For most data sets the exact information on the critical velocity (and corresponding pressure gradient) is generally not known.

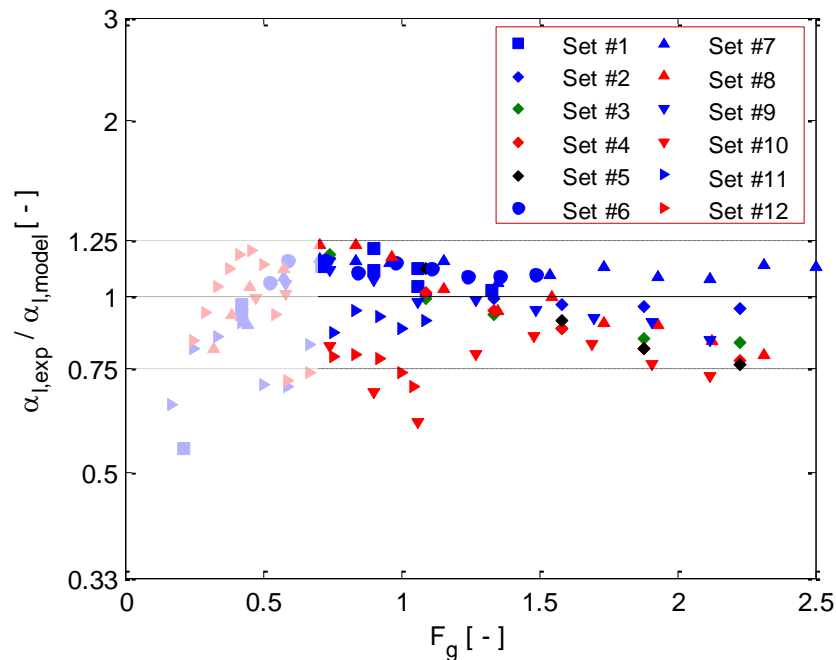


Figure 3.16 Experimental film holdup normalised with the model results for all air/water data sets. For $F_g < -0.8$ flow reversal occurs, where churn flow is expected to exist (blanked data).

In general, the film model tends to overpredict the pressure gradient for $F_g > 1$ by a maximum of about 20% (except for data set #10). For $0.75 < F_g < 1$, the model tends to underpredict the pressure gradient by a maximum of about 40% for the data sets #1 to #10 ($D = 34$ mm & 50 mm).

The data sets with $D = 80$ mm (sets #11 and #12), deviate differently from the film model results for $F_g < 1$. Since, for these two data sets, the deviation between the $f_{i,exp}$ and its model estimate is not much larger than for the other data sets, it seems that the turbulence effects are overestimated. Computing the pressure gradients with $A^+ = 500$ (i.e. neglecting turbulence) does decrease the model error for sets #11 and #12, but does also increase the overall deviation with the other data sets (especially data set #10).

For the film holdup, the deviations are larger than for the pressure gradient, but still fall roughly within the 25% error lines for all data sets for $F_g > 0.5$ as well (except for data set #12).

The onset of flow reversal occurs in the film model for $F_g = -0.8$. It is expected that for F_g lower than this value, churn flow exists where the film flow model may not describe the flow correctly anymore. Therefore, these data points are blanked.

3.5.2 Air/foam flows

In Figure 3.17 and Figure 3.18 are presented the experimental pressure gradient and film holdup normalised by the model predictions for all air/foam flows, respectively. The deviations of the model predictions to the experiments are significantly larger for the air/foam flows than for the air/water flows.

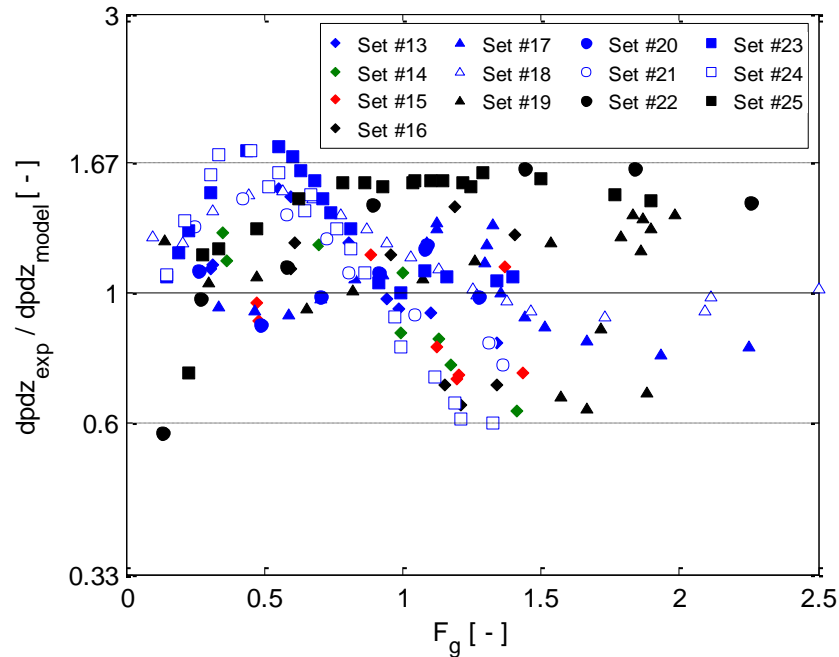


Figure 3.17 Experimental pressure gradient normalised with the model results for all air/foam data sets.

According to the film flow model, the onset of flow reversal with air/foam flows depends on surfactant concentration and liquid flow rate (see also Figure 3.19):

- With increasing liquid flow rate the film holdup increases as well. This results in a higher interfacial friction factor and higher actual gas core velocity, i.e. higher interfacial shear. Increasing the interfacial shear decreases the tendency for flow reversal.
- Increasing the surfactant concentration also has the tendency to increase the interfacial friction factor at high U_{sg} , hence tends to postpone the onset of flow reversal to lower values of F_g .

For some flow conditions, the onset of flow reversal occurs for F_g as low as 0.3.

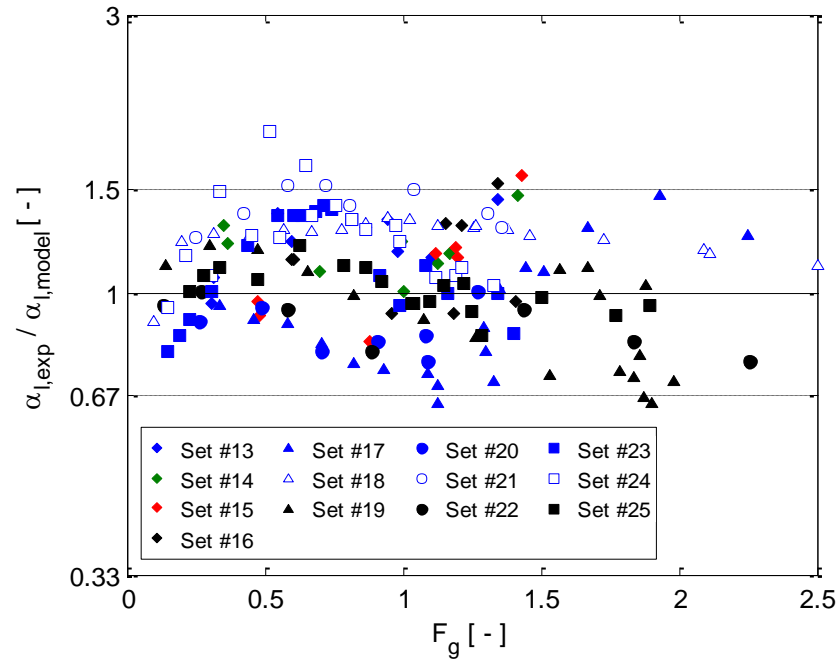


Figure 3.18 Experimental total liquid holdup normalised with the model results for all air/foam data sets.

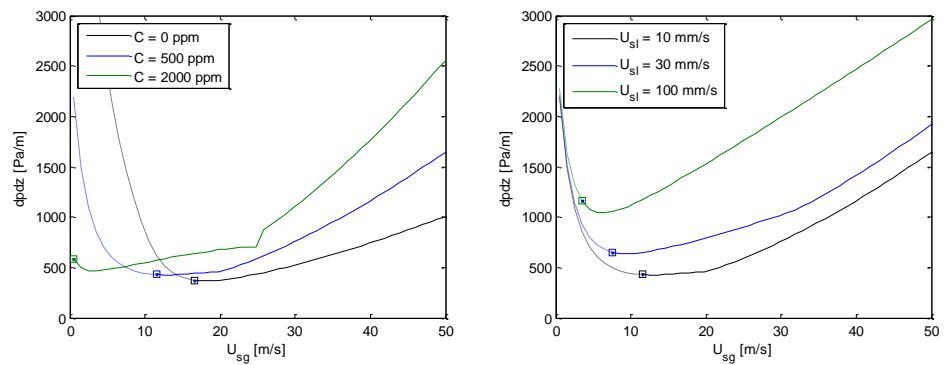


Figure 3.19 Pressure gradient as a function of gas velocity in a $D = 50$ mm pipe. Left graph: various Foamatron concentrations and constant liquid flow rate ($U_{sl} = 10$ mm/s). Right graph: various liquid flow rates and constant Foamatron concentration ($C = 500$ ppm). The square symbol indicates the onset of flow reversal.

4 Conclusions

The aim of this report is to develop a model that can predict the pressure drop for gas/liquid/foam pipe-flows under conditions that are relevant for gas wells up to the point of liquid loading. The added value of this newly developed model compared to the models that are already available in the literature and software tools, is the focus on the effect of adding surfactant to the flow, i.e. for Foam Assisted Lift.

A literature survey has been performed and revealed that the amount of experimental data on gas/liquid/foam flows is limited but most of the literature describe the effect of surfactants as postponing the transition from annular to churn flow to lower gas velocities due to the reduced density of the 'foamed liquid'. Therefore, a film flow model has been selected to describe gas/liquid/foam flows.

In sections 3.1 to 3.3 the film flow model with required closure relations have been set up. The closure relations have been deduced from experimental lab data, consisting of 12 air/water flow conditions and 13 air/foam flow conditions in three different flow setups.

The developed model is able to predict the pressure drop and liquid holdup of the experimental data set with a accuracy of ~25% for air/water flows and ~40% for air/foam flows for concurrent gas/liquid/foam flow conditions (i.e. above the liquid loading point). Such an accuracy is typical for software tools predicting multiphase flows. The choice of a film model to describe the flow thus is suitable.

Since the conditions at which the data sets are obtained differ significantly from field conditions (i.e. temperature, pressure and fluids), the closure relations deduced from these data sets may not be suitable for field conditions. On the other hand, at present it seems not feasible to perform flow tests for every unique condition that exists for each well to improve these closures, especially if multiple surfactants are to be tested. Therefore, a first step to develop a correlation between model parameters and 'easy' experiments has been proposed to enable the extrapolation to field conditions:

- The parameter A_T has been correlated to the carry-over tests in a Bikerman test setup. These tests are commonly performed to determine the performance of surfactants in combination with field fluids, and can approach field conditions.
- The viscosity of the liquid/foam film has been correlated to rheology measurements in an Anton Paar rheometer.

The model predicts a stronger dependency of the onset of flow reversal (liquid loading) on the liquid flow rate when surfactants are present.

5 Bibliography

- 1 Alamu, M.B., *Gas condensate well unloading critical rate*, SPE 166350, 2013.
- 2 Asali, J.C. et al, *Interfacial drag and film height for vertical annular flow*, AIChE J. 31(6), p 895-902, 1985.
- 3 Ashwood, A.C., et al., *A multiphase, micro-scale PIV measurement technique for liquid film velocity measurements in annular two-phase flow*, IJMF 68, pg 27-39, 2015.
- 4 Belfroid, S.P.C. et al, *Prediction Onset and Dynamic Behaviour of Liquid Loading Gas Well*, SPE 115567, 2008.
- 5 Belt, R.J., *On the liquid film in inclined annular flow*, PhD thesis, Delft University of Technology, 2007.
- 6 Blankenberger, P.L. et al, *Oil film behavior near the onset of flow reversal in immiscible gas/liquid vertical annular flow*, Int. Refrigeration and Air Conditioning Conf., paper 589, 2002.
- 7 Boer, J.P. de, *Deliquification Techniques – Best Practices*, TNO report OG-D-RPT-25319-001, 2011.
- 8 Breward, C.J.W., *The mathematics of foam*, PhD thesis, University of Oxford, 1999.
- 9 Christiansen, R.L., *A new look at foam for unloading gas wells*, R&D report Colorado School of Mines, 2006.
- 10 Coleman, *A new look at predicting gas well load-up*, SPE 20280, 1991.
- 11 Dalland, M. and Hanssen, J.E., *GOR-Control foams: demonstration of oil-based foam process efficiency in a physical flow model*, SPE 50755, 1999.
- 12 Deshpande, N.S. and Barigou, M., *The flow of gas-liquid foams through pipe fittings*, Int J Heat Fluid Flow 22, p 94-101, 2001.
- 13 Gylys, J. et al, *Vertical channel's heat transfer to the upward foam flow*, Int J Heat and Mass Transfer, 83, p 465-478, 2015.
- 14 Dousi, N. et al, *Numerical and analytical modeling of the gas-well liquid loading process*, SPE 95282, p 475-482, 2006.
- 15 Flores-Avila, F. S. et al, *Experimental evaluation of control fluid fallback during off-bottom well control Effect of deviation angle*, SPE 74568, 2002.
- 16 Fore, L.B. et al, *Interfacial friction in gas-liquid annular flow: analogies to full and transition roughness*, IJMF 26, p 1755-1799, 2000.
- 17 Geusgens, J.T.V.M., *Schuimtransport in een verticale pijp (in Dutch)*, R&D Scheikundige Technologie, Hogeschool Eindhoven, 1964.
- 18 Hanratty, T.J., *Physics of Gas-Liquid Flows*, Cambridge, UK, ISBN 978-1-107-04120-2, 2013.
- 19 Hewitt, G.F., *Co-current and countercurrent two phase annular flow*, 9th Australasian Fluid Mechanics Conf., 1986.
- 20 Herzhaft, B. *Rheology of aqueous foams: a literature review of some experimental works*, Oil & Gas Sci. and Techn. 54(5), p 587-596, 1999.
- 21 Kawale, D., *Influence of dynamic surface tension on foams: application in gas well deliquification*, MSc TUDelft, 2011.
- 22 Kelly, C. and Shearer, V., *Gas well deliquification using foamers*, 7th EGWDC, short course by Clariant, 2012.
- 23 Kroezen, A.B.J., et al, *The flow properties of foam*, JSDC, 104, p 393-400, 1988.
- 24 Lea, J.F. et al, *Gas well deliquification*, pp. 193-240, 2008.

- 25 Li, H. et al, *Theoretical model for optimizing surfactant usage in a gas well dewatering process*, PETSOC 2007(118).
- 26 Liu, L. et al, *Effect of surfactant additive on vertical two-phase flow*, J. Petr. Sci. Eng. 115, p 1-10, 2014.
- 27 Loillier, P., *Numerical Simulation of Two-phase gas-liquid flows in inclined and vertical pipelines*, PhD thesis, Cranfield University, 2006.
- 28 Lumban-Gaol, A. and Valko, P.P., *Liquid holdup correlation for conditions affected by partial flow reversal*, IJMF 67, p 149-159, 2014.
- 29 Luo, S. et al, *A new comprehensive model for predicting liquid loading in gas wells*, SPE 172501, 2014.
- 30 McQuillan, K.W. et al, *Flooding in vertical two-phase flow*, IJMF 11(6), p 741-760, 1985.
- 31 Meulen, G.P. van der, *Churn-annular Gas-liquid flows in large diameter vertical pipes*, PhD thesis (TMF4/P310(12)), University of Nottingham, 2012.
- 32 Mitchell, B.J., *Viscosity of foam*, PhD thesis, University of Oklahoma, 1970.
- 33 Moalem Maron, D. and Dukler, A.E., *Flooding and upward film flow in vertical tubes – II*, IJMF 10(5) p 599-621, 1984.
- 34 Nimwegen, A. v. et al, *A first look at the hydrodynamics of air-water-foam flow for gas well deliquification*, BHR Multiphase Flow Technology 8, Cannes, p. 1-14, 2012.
- 35 Nimwegen, A. v. et al, *The Effect of Surfactants on Vertical Air/Water Flow for Prevention of Liquid Loading*, SPE 164095, 2013.
- 36 Nimwegen, A. v. et al, *Experiments on surfactants for gas well deliquification in vertical pipes with different diameters*, EGWDC 2014.
- 37 Nimwegen, A. v. et al, *The effect of surfactants on air-water annular and churn flow in vertical pipes. Part 1: Morphology of the air-water interface*, IJMF 71, p 133-145, 2015.
- 38 Nimwegen, A. v. et al, *The effect of surfactants on air-water annular and churn flow in vertical pipes. Part 2: Liquid holdup and pressure gradient dynamics*, IJMF 71, p 146-158, 2015.
- 39 Nimwegen, A.T. van, *The effect of Surfactants on Gas-Liquid Pipe Flows*, PhD thesis, Delft University of Technology, 2015.
- 40 Omebere-Iyari, N.K. et al, *The characteristics of gas/liquid flow in large risers at high pressures*, IJMF 34, p 461-476, 2008.
- 41 Oude Heuvel, S. and Adelizzi, C., *Gas well deliquification by chemical foam*, 8th EGWDC, short course by Nalco Champion, 2013.
- 42 Pakulski, M. *Testing gas well deliquification chemicals at real downhole conditions*, SPE 121564, 2009.
- 43 Skopich, A., et al, *Pipe diameter effect on liquid loading in vertical gas wells*, SPE production and operations symposium, SPE164477, 2013.
- 44 Soni, S., Kelkar, M., *Pressure-drop predictions in tubing in the presence of surfactants*, SPE 120042, 2009.
- 45 Turner, R.G., et al, *Analysis and Prediction of Minimum Flow Rate for the Continuous Removal of Liquids from Gas wells*, Journal of Petroleum Technology, 246, pp 1476-1482, 1969.
- 46 Veeken, K, et al, *Gas well liquid loading field data analysis and multiphase flow modelling*, SPE Prod & Operations, 2010.
- 47 Veeken, K. et al, *Transient multiphase flow modeling of gas well liquid loading*, SPE 123657, 2009.
- 48 Weaire, D., *The rheology of foam*, Colloid and Interface Sci 13, p 171-176, 2008.

- 49 Westende, J.M.C. van 't, *Droplets in annular-dispersed gas-liquid pipe-flows*, PhD thesis, Delft University of Technology, 2008.
- 50 Yang, J. et al, *Foam for gas well deliquification*, Colloids and Surfaces A: Physicochem. Eng. Aspects 309, p177-181, 2007.
- 51 Yang, J. et al, *Effect of dynamic surface activity of surfactant on performance of foam for gas well deliquification*, SPE-165366, 2013.
- 52 Yuan, G. et al, *An experimental study on liquid loading of vertical and deviated gas wells*, SPE 164516, 2013.
- 53 Zabaras, G. et al, *Vertical upward concurrent gas-liquid annular flow*, AIChE J. 32(5), p 829-843, 1986.
- 54 Zabaras, G. and Dukler, A.E., *Countercurrent gas-liquid annular flow, including the flooding state*, AIChE J. 34(3), p 389-396, 1988.
- 55 Zhou, J., *Flow patterns in vertical air/water flow with and without surfactant*, MSc thesis, University of Dayton, 2013.

6 Signature

Delft, 17 December 2015



Garrelt Alberts
Manager HTFD

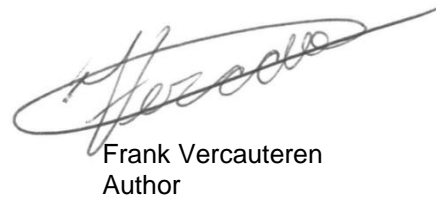
TNO



Jos van 't Westende
Author



Jordy de Boer
Author



Frank Vercauteren
Author

A Symbol list

Table A.1 List of symbols

Symbol	Unit	Description
A^+	-	Van Driest constant
A_r	-	Horizontal asymptote in foam quality closure
C	ppm	Surfactant concentration
C_{min}	-	Minimum effective surfactant concentration
CMC		Critical Micelle Concentration
CO_{tot}	-	Relative total carry-over in small scale Bikerman test
D	m	Pipe diameter
d_f	m	Film thickness
$d_{f,crit}$	m	Critical film thickness for waves to appear
$d_{f,0}$	m	Vertical asymptote in foam quality closure
d_μ	m	Viscous length scale
FAL		Foam Assisted Lift
F_g	-	Densimetric gas-phase Froude number
f_G	-	Fanning friction factor (Blasius)
f_i	-	Interfacial friction factor
g	m/s ²	Gravitational acceleration
JIP		Joint Industry Project
l_m	m	Mixing length
P	Pa	Pressure
$\nabla_z p, dpdz$	Pa/m	Pressure gradient along axial direction
r	m	Radial coordinate
Re_{sg}	-	Gas phase Reynolds number based on superficial velocity
S	m	Circumference of a circle
TPC		Tubing Performance Curve
u	m/s	Local film velocity
U_{sg}	m/s	Superficial gas velocity
U_{sl}	m/s	Superficial liquid velocity
$U_{sl,model}$	m/s	Superficial liquid velocity as predicted by the film model
$U_{sl,exp}$	m/s	Superficial liquid velocity as measured in the experiments
u_τ	m/s	Friction velocity
y	m	Distance to the wall
z	m	Axial coordinate
α_f	-	Film holdup
α_l	-	Liquid holdup
β	-	Coefficient used in eq. 3.18
γ	-	Coefficient used in eq. 3.15 and 3.18
Γ	-	Foam quality
$\langle \Gamma_f \rangle$	-	Mean film quality
Γ_f	-	Local film quality
κ	-	Von Karman constant
μ_f	Pa s	Film viscosity
$\mu_{f,model}$	Pa s	Film viscosity computed by film model
$\mu_{f,tot}$	Pa s	Local total film viscosity
μ_τ	Pa s	Apparent turbulent viscosity
μ_l	Pa s	Liquid viscosity

ρ_f	Kg/m3	Film density
ρ_g	Kg/m3	Gas density
ρ_l	Kg/m3	Liquid density
τ	Pa	Shear stress
τ_c	Pa	Characteristic shear stress for wall-bounded turbulence
τ_i	Pa	Interfacial shear stress
τ_w	Pa	Wall shear stress

B Film flow

Film flow is characterised in this report by the shear stress profile and velocity profile. They are linked via the viscosity : eq. 3.2. For Newtonian fluids, the viscosity is constant and the following extreme conditions can be identified :

- Uniform upflow
- Onset of flow reversal
- Zero net flow
- Onset of flooding
- Free falling film

In the flow regime between the onset of flow reversal and the onset of flooding the film shows partial upflow and partial downflow. Under these conditions the boundary conditions have a large effect on the flow behaviour.

B.1 Uniform upflow

With uniform upflow the interfacial shear stress is sufficiently high that the wall shear is positive, i.e. $0 < \tau_w < \tau_i$. The velocity is positive at all locations in the film.

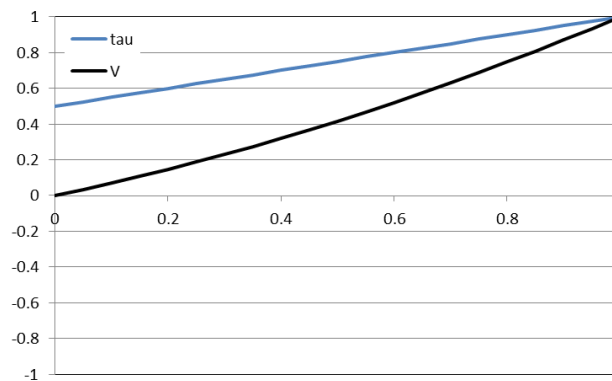


Figure B.1 Shear stress (blue) and velocity profile (black) for upward annular flow as a function of the normalised distance to the wall (y/d_i). The shear stress (τ) and velocity (V) are both normalised by its maximum value.

B.2 Onset of flow reversal

With flow reversal the interfacial shear stress is such that the wall shear stress is zero, i.e. $0 = \tau_w < \tau_i$. The velocity is just positive at all locations in the film. In laboratory experiments the onset of flow reversal marks the condition for which there does not appear any liquid below the liquid feed.

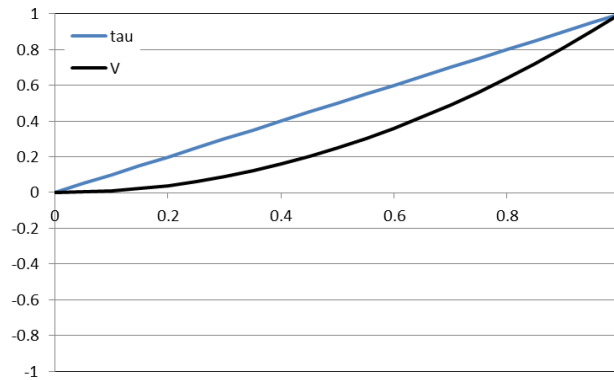


Figure B.2 Shear stress (blue) and velocity profile (black) at the onset of flow reversal as a function of the normalised distance to the wall (y/d_i). The shear stress (τ) and velocity (V) are both normalised by its maximum value.

B.3 Zero net flow

With zero net flow the amount of upflow equals that of downflow. For Newtonian fluids this holds for : $\tau_w = -\tau_i / 2$.

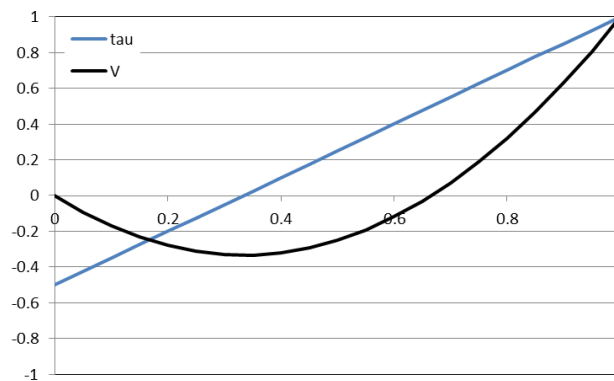


Figure B.3 Shear stress (blue) and velocity profile (black) at zero net flow as a function of the normalised distance to the wall (y/d_i). The shear stress (τ) and velocity (V) are both normalised by its maximum value.

B.4 Onset of flooding

At the onset of flooding the interfacial shear stress is such that the film velocity is just negative at all locations in the film. This holds for: $\tau_w = -\tau_i$. In laboratory experiments the onset of flooding marks the condition for which there does not appear any liquid above the liquid feed.

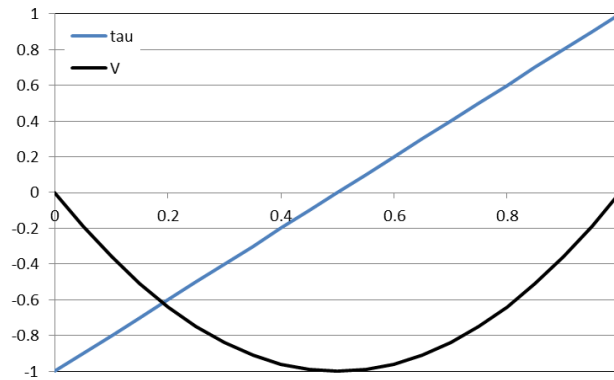


Figure B.4 Shear stress (blue) and velocity profile (black) at the onset of flooding as a function of the normalised distance to the wall (y/d_i). The shear stress (τ) and velocity (V) are both normalised by its maximum value.

B.5 Free falling film

A free falling film flow is characterized by: $\tau_w < \tau_i = 0$. The velocity is negative at all locations in the film.

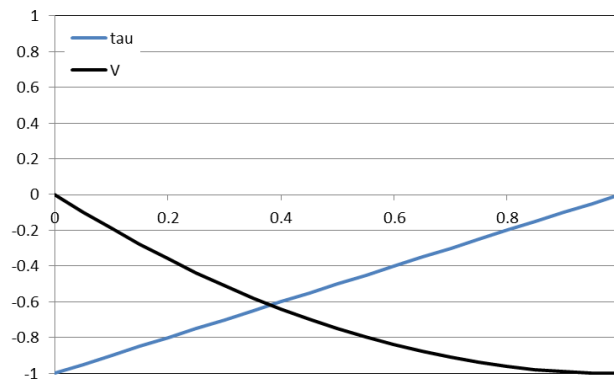


Figure B.5 Shear stress (blue) and velocity profile (black) for a free falling film as a function of the normalised distance to the wall (y/d_i). The shear stress (τ) and velocity (V) are both normalised by its maximum value.

B.6 Partial upflow / partial downflow

For $\tau_i / 2 < -\tau_w < \tau_i$ there can exist both upflow and downflow in the liquid film. In this range Moalem-Maron (ref. 33) found two solutions to the combined mass and momentum balance :

- Circulating flow : the net upflow equals the liquid feed rate. This means that liquid may temporarily flow downward, but eventually will be transported upwards, i.e. there is no drainage of liquid at the upstream side of the tubing.
- Split flow : the sum of the upflow and the (absolute value of) the downflow equals the liquid feed rate. This means that there exist two 'flow paths' which hardly interfere : one going up and one going down. For this solution to be sustainable, drainage at the upstream side must be sufficient to prevent downhole accumulation.

Both for the experimental data sets that the model is developed for as well as the typical conditions at which liquid loading occurs, the drainage at the downhole side is limited and the circulating flow solution is most appropriate.

B.7 Film turbulence

Ashwood et al have performed detailed PIV measurements of the velocity in the liquid film of an air/water upward annular flow. The experimental setup consisted of a rectangular duct with dimensions 33.0mm x 20.3mm (hydraulic diameter = 25.1mm). These measurements have been used to estimate the relevant turbulent film flow parameter (i.e. the van Driest constant : A^+) that can predict these experiments.

The turbulent velocity profile is determined via the integration of the local velocity gradient, which is taken as the ratio of the local shear stress over the local effective viscosity ($du/dy = \tau/\mu_{\text{eff}}$). The effective viscosity is the sum of the fluid viscosity and the apparent turbulent viscosity (the latter is computed using mixing length theory and van Driest wall damping (see section 3.3.2)). The shear stress increases with distance from the wall due to the weight of the liquid ¹⁵ : $\tau(y) = \tau_w + \rho_L g y$. The wall shear is taken equal to Ashwoods estimate via the PIV measurements. The friction velocity that is needed for the turbulent apparent viscosity measurement is calculated via a characteristic stress: $\tau_c = \tau(d_f / 3)$, where the film thickness, d_f , is taken equal to the largest distance to the wall of the data set.

In Figure B.6 the results of the calculated turbulent velocity profile is shown together with the corresponding data set. A van Driest constant of $A^+ = 150$ seems to represent the data reasonably well.

¹⁵ This deviates from the assumption used in Ashwood et al.

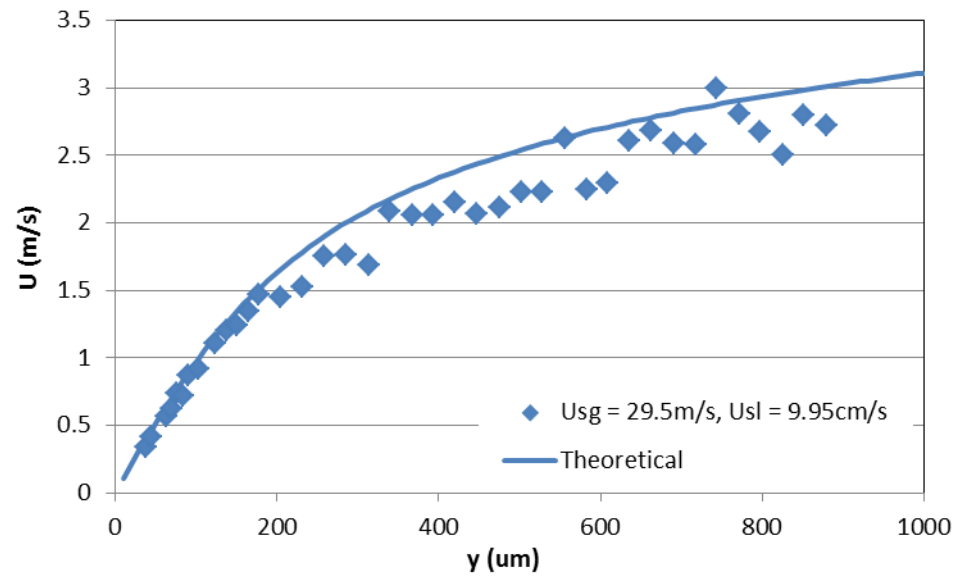


Figure B.6 Velocity profile measurements of a turbulent liquid film in an upward annular flow by Ashwood et al. (2015). The solid line represents a theoretical fit calculated via the integration of the local velocity gradient using : $\tau_w = 10.3\text{Pa}$, $d_f = 880\mu\text{m}$, $\tau_c = 13.2\text{Pa}$ and $A^+ = 150$.

C Experimental data

Section C.1 presents a description of the flow loop setup with which the majority of the data sets are obtained (all except Set #10).

Sections C.2 to C.26 present all experimental data sets that have been used in the modelling in table format. In case the index number (first column of the tables) is italic/underlined this means that the wall shear stress is negative (flow reversal). Italic/underlined values for d_{pdz} , α_f or α_L (columns 3 to 5 of the tables) indicate that these are interpolated values.

The results of the film flow model are shown in the sections C.1 to C.25 as well in graph format. Each graph shows the following: top left : Γ_{film} vs d_f/D , top middle : μ_{film} vs Γ_{film} , top right : $f_{i,exp}$ vs d_f/D , bottom left : α_{film} vs U_{sg} , bottom middle : α_l vs U_{sg} , bottom right : d_{pdz} vs U_{sg} .

The table below presents an overview the characteristics of all data sets.

Table C.1 Datasets used for modelling

Set	Symbol	U_{sl} [mm/s]	C [ppm]	Surfactant	D [mm]	Author
1	■	10	0	-	50	TNO
2	◆	10	0	-	50	Belt/Westende
3	◆	20	0	-	50	Belt/Westende
4	◆	40	0	-	50	Belt/Westende
5	◆	80	0	-	50	Belt/Westende
6	●	10	0	-	50	Ajani
7	▲	10	0	-	34	Nimwegen
8	▲	50	0	-	34	Nimwegen
9	▼	10	0	-	50	Nimwegen
10	▼	50	0	-	50	Nimwegen
11	▶	10	0	-	80	Nimwegen
12	▶	50	0	-	80	Nimwegen
13	◆	10	200	Foamatron	50	TNO
14	◆	10	500	Foamatron	50	TNO
15	◆	10	1000	Foamatron	50	TNO
16	◆	10	2000	Foamatron	50	TNO
17	▲	10	1000	Trifoam	34	Nimwegen
18	▲	50	1000	Trifoam	34	Nimwegen
19	▲	10	3000	Trifoam	34	Nimwegen
20	●	10	1000	Trifoam	50	Nimwegen
21	○	50	1000	Trifoam	50	Nimwegen
22	●	10	3000	Trifoam	50	Nimwegen
23	■	10	1000	Trifoam	80	Nimwegen
24	□	50	1000	Trifoam	80	Nimwegen
25	■	10	3000	Trifoam	80	Nimwegen

C.1 Flow experimental setup

C.1.1 Dimensions

The large scale flow loop used for the measurements is similar to that used in the PhD of Dries van Nimwegen, located at the (former) “Kramers Laboratorium voor Fysische Technologie” (ref. 39, see Figure C.1). His 50 mm ID setup has been used for obtaining additional measurements. This setup consist of a 12 m vertical acrylic pipe, built out of sections with varying length (in the range of 0.3 m to 1 m length). All pipe sections are interconnected using flanges and are machined to ensure smooth transition.



Figure C.1 Picture of the TUDelft Flow Loop

C.1.2 Flow control

Dry air is flowing into the setup at the bottom, and is released to atmosphere at the top of the setup. The air flow is regulated using a mass flow controller (Mass-Stream D6383, M+W Instruments (Bronkhorst)) with a range of 0-5000 l/min (at standard conditions), and an accuracy of 2% of full scale.

Liquid is injected into the system through approximately 1m ($\sim 20L/D$) downstream of the gas inlet. The liquid is injected through an annulus thereby creating a liquid film at the wall. The liquid is dragged by the air flow to the top of the pipe where it is separated from the air stream in a separator. In the open loop configuration (only used with air/water flows), the liquid from the separator is drained to the sewer.

When the system is in the closed loop configuration the liquid is collected in a large tank ($\sim 2 \text{ m}^3$ volume) from which it is reinjected in the system. The liquid flow rate is measured via a magnetic flow meter (Mag-View MVM020, Massflow-online (Bronkhorst)) with a range of 1-20 l/min and an accuracy of 2% of reading. The flow is regulated using a valve, which is controlled using a PID.

C.1.3 *Measurements*

Two fast closing ball valves are used to shut-in the liquid/foam flow over a length of 3.99 m pipe; this is done during a holdup measurement. The bottom valve is located about 7 m ($\sim 140L/D$) downstream of the liquid feed. Directly after shut-in of the liquid/foam flow (i.e. before foam collapse), the volume of the liquid + foam is measured, which gives the value for α_f . After waiting for about 30 mins, all foam has collapsed (or most liquid has drained out of the foam) and the volume of the liquid below the foam is measured, which gives the value for α_l .

Two pressure transducers are used to estimate the pressure gradient over a distance of 1.96 m. The bottom transducer is located about 8.5 m downstream of the liquid feed (i.e. both pressure transducers are in between the two fast closing valves).

C.1.4 *Mixture*

In case a surfactant mixture was tested in the setup, a master solution was prepared initially in a small portable vessel. The amount of water and surfactant for this master solution was measured on a scale with an accuracy of 0.1 g. Hereafter, the master solution is poured into the large tank and mixed with an additional amount of water in order to obtain a specific surfactant concentration. The error in surfactant concentration is estimated to be less than ~ 0.02 ppm (based on a dead volume of the master solution vessel of 0.05 L and master solution volumes of at least 3 L).

Two surfactants have been tested, which are referred to as Foamatron and Trifoam.

- Trifoam : Trifoam 820 Block, Oilchem GmbH, Dessau-Rosslau, Germany.
- Foamatron : Foamatron V505, Ethanediol (30% , <60%), dimethyl-3-propylammonium hydroxide (10% , <25), Nalco-Champion, The Netherlands.

C.2 Set #1

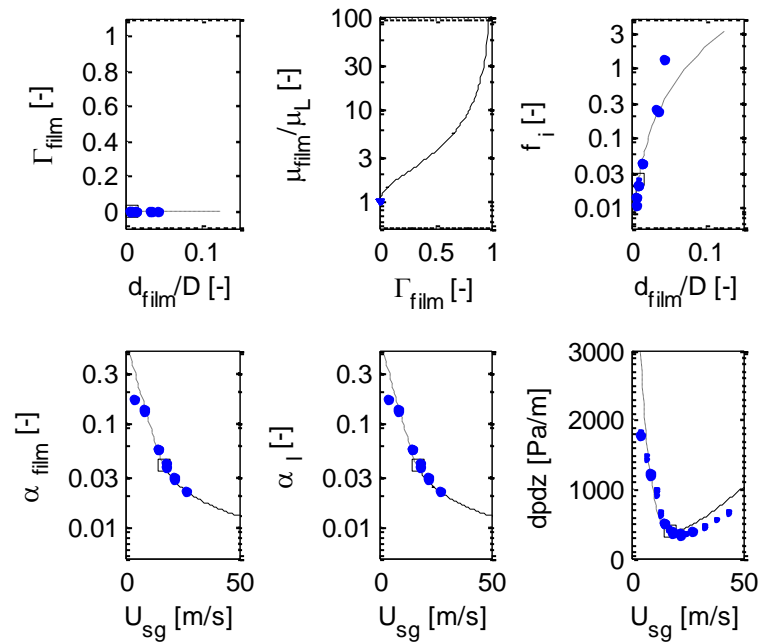


Figure C.2 $D = 50$ mm, $U_{sl} = 10$ mm/s, $C = 0$ ppm, TNO (2015)

Table C.2 $D = 50$ mm, $U_{sl} = 10$ mm/s, $C = 0$ ppm, TNO (2015)

#	U_{sg} (m/s)	dp/dz (Pa/m)	α_f (-)	α_L (-)
1.01	4.29	1771.1	0.1666	0.1666
<u>1.02</u>	8.59	1208.4	0.1363	0.1363
<u>1.03</u>	8.59	1235.4	0.1314	0.1314
<u>1.04</u>	14.49	506.0	0.0567	0.0567
<u>1.05</u>	14.49	509.5	0.0563	0.0563
<u>1.06</u>	18.25	367.8	0.0405	0.0405
1.07	18.25	379.5	0.0372	0.0372
1.08	21.47	345.8	0.0302	0.0302
1.09	21.47	347.9	0.0281	0.0281
1.10	26.83	391.5	0.0219	0.0219

C.3 Set #2

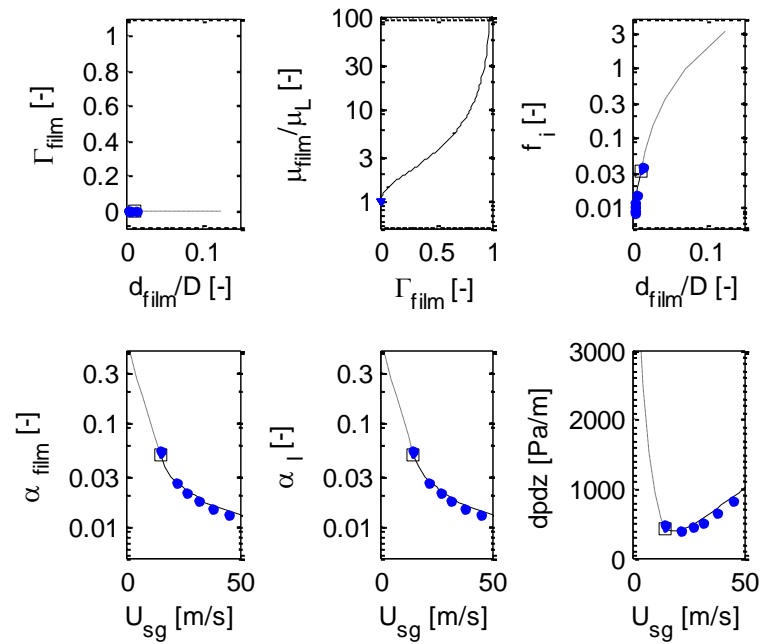


Figure C.3 $D = 50 \text{ mm}$, $U_{\text{sl}} = 10 \text{ mm/s}$, $C = 0 \text{ ppm}$, Westende/Belt (2006)

Table C.3 $D = 50 \text{ mm}$, $U_{\text{sl}} = 10 \text{ mm/s}$, $C = 0 \text{ ppm}$, Westende/Belt (2006)

#	U_{sg} (m/s)	dp/dz (Pa/m)	α_f (-)	α_L (-)
2.01	15.00	486.9	0.0544	0.0544
2.02	22.00	383.0	0.0266	0.0266
2.03	27.00	436.3	0.0211	0.0211
2.04	32.00	517.8	0.0175	0.0175
2.05	38.00	639.6	0.0150	0.0150
2.06	45.00	817.6	0.0130	0.0130

C.4 Set #3

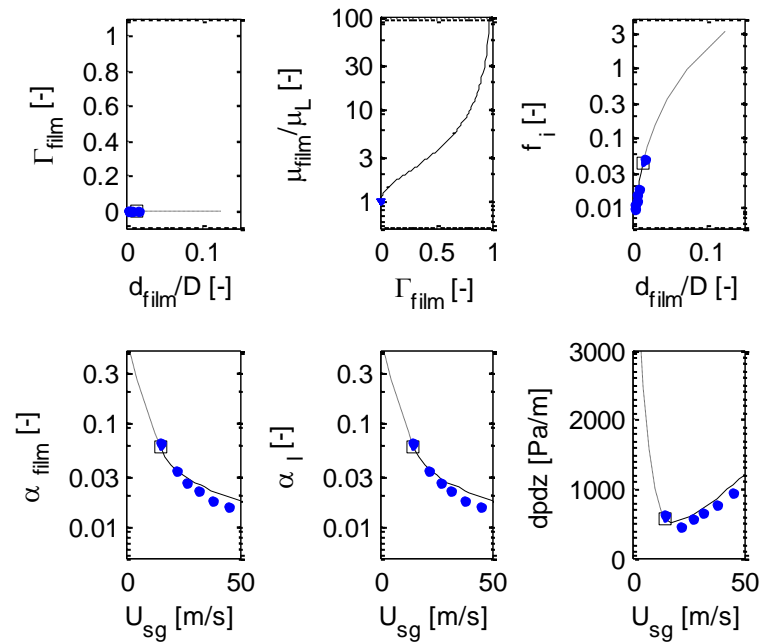


Figure C.4 $D = 50$ mm, $U_{sl} = 20$ mm/s, $C = 0$ ppm, Westende/Belt (2006)

Table C.4 $D = 50$ mm, $U_{sl} = 20$ mm/s, $C = 0$ ppm, Westende/Belt (2006)

#	U_{sg} (m/s)	dp/dz (Pa/m)	α_f (-)	α_L (-)
3.01	15.00	619.8	0.0649	0.0649
3.02	22.00	460.6	0.0339	0.0339
3.03	27.00	557.1	0.0263	0.0263
3.04	32.00	644.5	0.0216	0.0216
3.05	38.00	772.5	0.0179	0.0179
3.06	45.00	928.9	0.0155	0.0155

C.5 Set #4

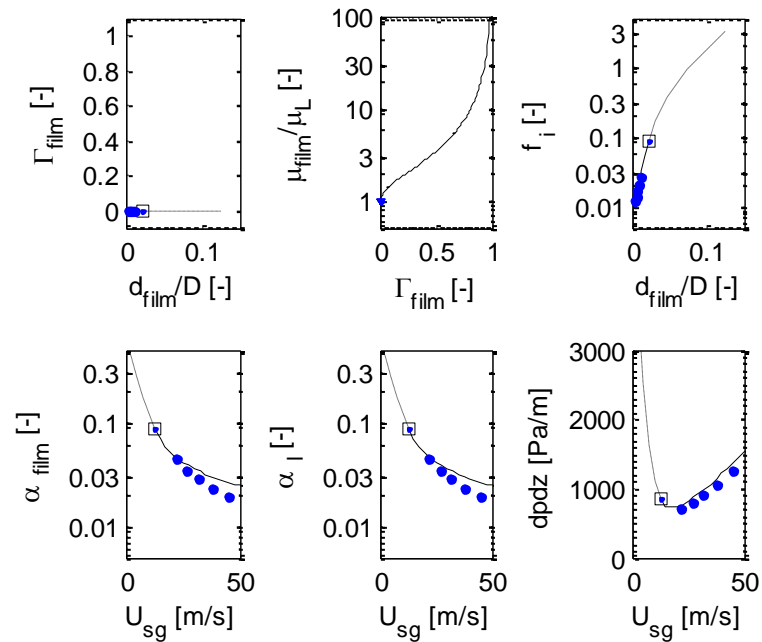


Figure C.5 $D = 50 \text{ mm}$, $U_{\text{sl}} = 40 \text{ mm/s}$, $C = 0 \text{ ppm}$, Westende/Belt (2006)

Table C.5 $D = 50 \text{ mm}$, $U_{\text{sl}} = 40 \text{ mm/s}$, $C = 0 \text{ ppm}$, Westende/Belt (2006)

#	U_{sg} (m/s)	dp/dz (Pa/m)	α_f (-)	α_L (-)
4.01	22.00	701.9	0.0446	0.0446
4.02	27.00	791.5	0.0350	0.0350
4.03	32.00	897.5	0.0285	0.0285
4.04	38.00	1050.5	0.0232	0.0232
4.05	45.00	1255.5	0.0197	0.0197

C.6 Set #5

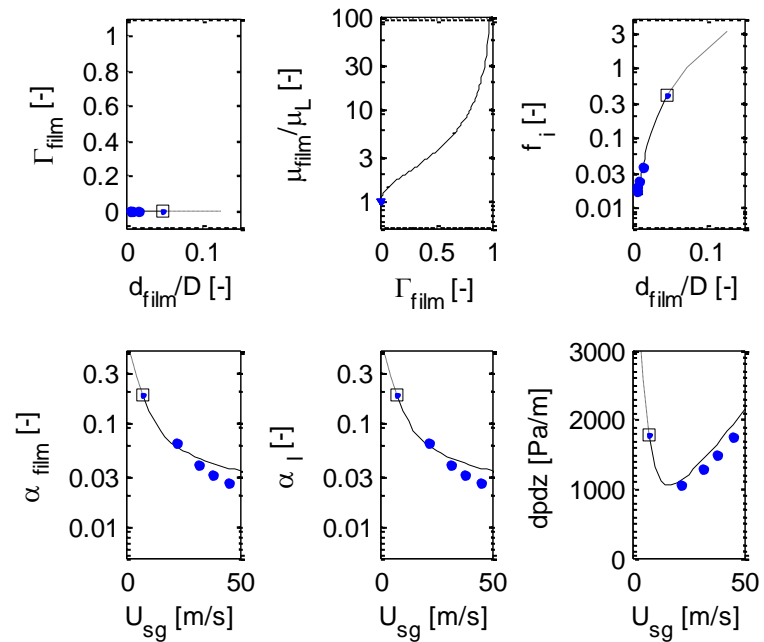


Figure C.6 $D = 50$ mm, $U_{\text{sl}} = 80$ mm/s, $C = 0$ ppm, Westende/Belt (2006)

Table C.6 $D = 50$ mm, $U_{\text{sl}} = 80$ mm/s, $C = 0$ ppm, Westende/Belt (2006)

#	U_{sg} (m/s)	dp/dz (Pa/m)	α_f (-)	α_L (-)
5.01	22.00	1046.1	0.0630	0.0630
5.02	32.00	1287.4	0.0391	0.0391
5.03	38.00	1476.0	0.0311	0.0311
5.04	45.00	1751.2	0.0261	0.0261

C.7 Set #6

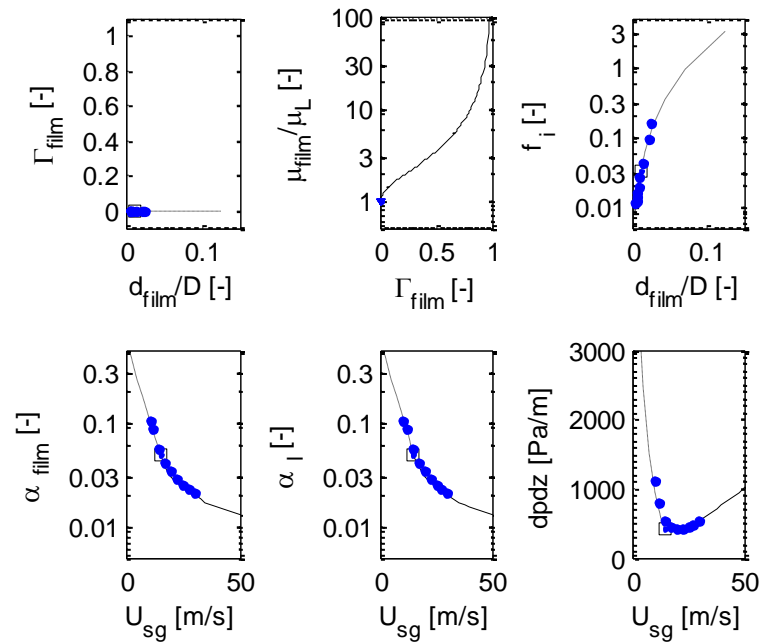


Figure C.7 $D = 50$ mm, $U_{sl} = 10$ mm/s, $C = 0$ ppm, Ajani (2014)

Table C.7 $D = 50$ mm, $U_{sl} = 10$ mm/s, $C = 0$ ppm, Ajani (2014)

#	U_{sg} (m/s)	dp/dz (Pa/m)	α_f (-)	α_L (-)
6.01	10.60	1104.1	0.1017	0.1017
6.02	11.94	796.2	0.0860	0.0860
6.03	14.67	524.7	0.0560	0.0560
6.04	17.13	433.1	0.0407	0.0407
6.05	19.80	416.1	0.0342	0.0342
6.06	22.48	430.3	0.0286	0.0286
6.07	25.05	454.9	0.0248	0.0248
6.08	27.45	489.1	0.0226	0.0226
6.09	30.07	547.0	0.0209	0.0209

C.8 Set #7

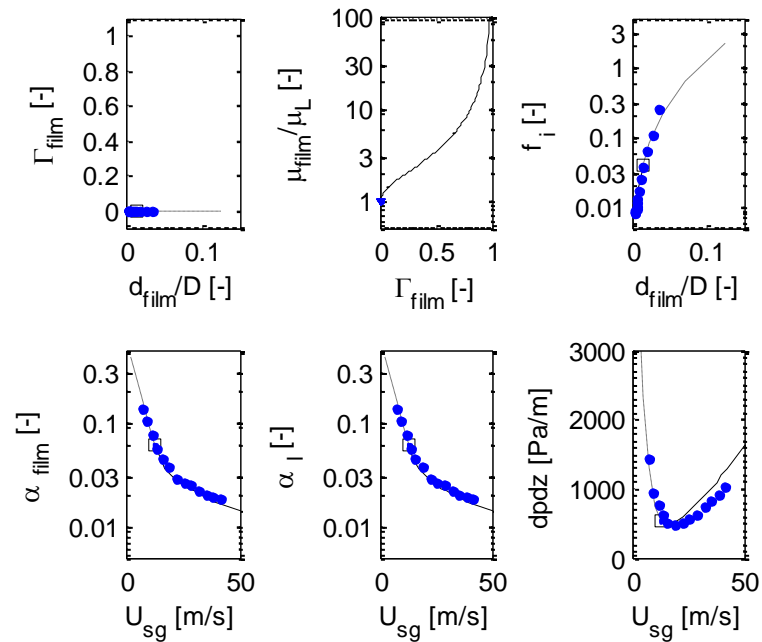


Figure C.8 $D = 34$ mm, $U_{\text{sl}} = 10$ mm/s, $C = 0$ ppm, Nimwegen (2015)

Table C.8 $D = 34$ mm, $U_{\text{sl}} = 10$ mm/s, $C = 0$ ppm, Nimwegen (2015)

#	U_{sg} (m/s)	dp/dz (Pa/m)	α_f (-)	α_L (-)
7.01	7.47	1431.7	0.1382	0.1382
<u>7.02</u>	9.58	941.4	0.1058	0.1058
<u>7.03</u>	11.77	757.4	0.0763	0.0763
7.04	13.95	606.8	0.0562	0.0562
7.05	16.03	514.9	0.0456	0.0456
7.06	19.26	490.1	0.0370	0.0370
7.07	22.51	511.5	0.0289	0.0289
7.08	25.70	562.2	0.0263	0.0263
7.09	28.93	633.8	0.0246	0.0246
7.10	32.15	722.3	0.0216	0.0216
7.11	35.32	823.3	0.0199	0.0199
7.12	38.55	915.9	0.0195	0.0195
7.13	41.77	1037.9	0.0182	0.0182

C.9 Set #8

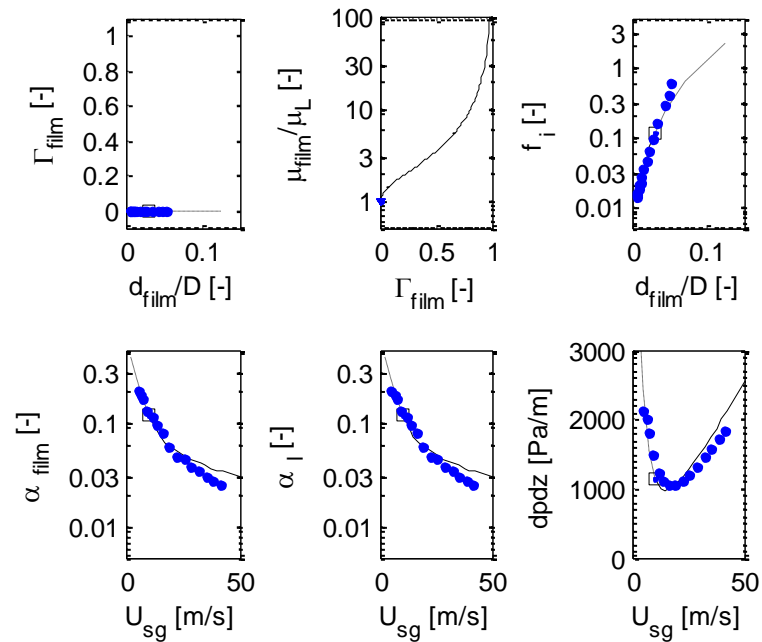


Figure C.9 $D = 34$ mm, $U_{sl} = 50$ mm/s, $C = 0$ ppm, Nimwegen (2015)

Table C.9 $D = 34$ mm, $U_{sl} = 50$ mm/s, $C = 0$ ppm, Nimwegen (2015)

#	U_{sg} (m/s)	dp/dz (Pa/m)	α_f (-)	α_L (-)
8.01	5.34	2129.9	0.1997	0.1997
8.02	6.43	1995.8	0.1861	0.1861
8.03	7.52	1803.1	0.1707	0.1707
8.04	9.63	1472.1	0.1323	0.1323
8.05	11.81	1229.1	0.1122	0.1122
8.06	13.92	1111.7	0.0938	0.0938
8.07	16.08	1053.1	0.0780	0.0780
8.08	19.27	1048.9	0.0588	0.0588
8.09	22.52	1107.5	0.0477	0.0477
8.10	25.72	1199.7	0.0456	0.0456
8.11	28.95	1312.8	0.0379	0.0379
8.12	32.18	1446.9	0.0349	0.0349
8.13	35.39	1568.4	0.0306	0.0306
8.14	38.57	1702.5	0.0272	0.0272
8.15	41.79	1824.0	0.0255	0.0255

C.10 Set #9

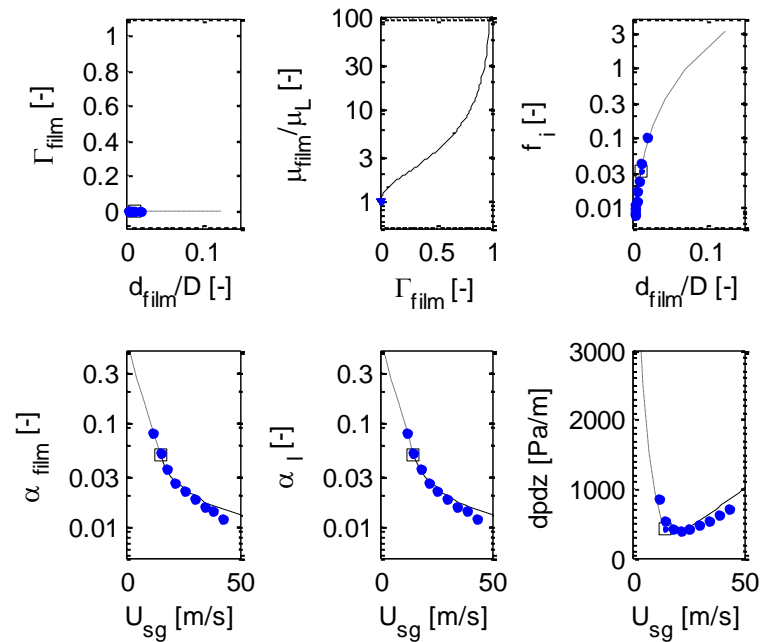


Figure C.10 $D = 50 \text{ mm}$, $U_{\text{sl}} = 10 \text{ mm/s}$, $C = 0 \text{ ppm}$, Nimwegen (2015)

Table C.10 $D = 50 \text{ mm}$, $U_{\text{sl}} = 10 \text{ mm/s}$, $C = 0 \text{ ppm}$, Nimwegen (2015)

#	U_{sg} (m/s)	dp/dz (Pa/m)	α_f (-)	α_L (-)
9.01	11.79	860.5	0.0808	0.0808
9.02	15.01	523.6	0.0515	0.0515
9.03	18.21	420.0	0.0359	0.0359
9.04	21.44	399.8	0.0265	0.0265
9.05	25.74	429.8	0.0219	0.0219
9.06	30.03	484.7	0.0181	0.0181
9.07	34.28	548.0	0.0156	0.0156
9.08	38.59	632.1	0.0140	0.0140
9.09	42.90	720.4	0.0119	0.0119

C.11 Set #10

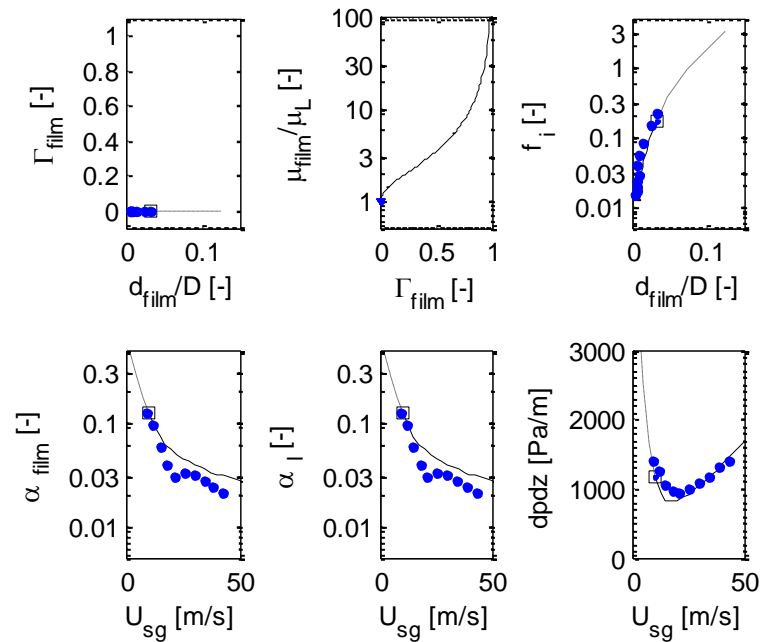
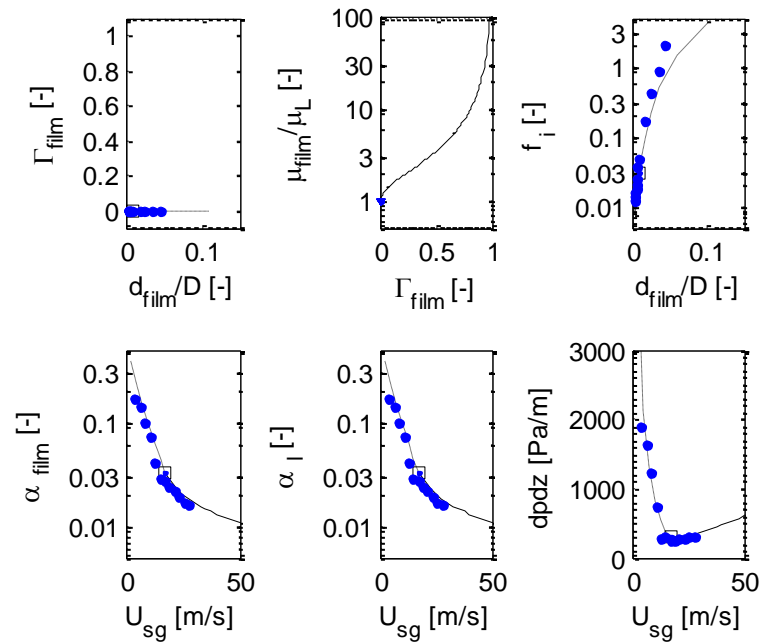


Figure C.11 $D = 50$ mm, $U_{\text{sl}} = 50$ mm/s, $C = 0$ ppm, Nimwegen (2015)

Table C.11 $D = 50$ mm, $U_{\text{sl}} = 50$ mm/s, $C = 0$ ppm, Nimwegen (2015)

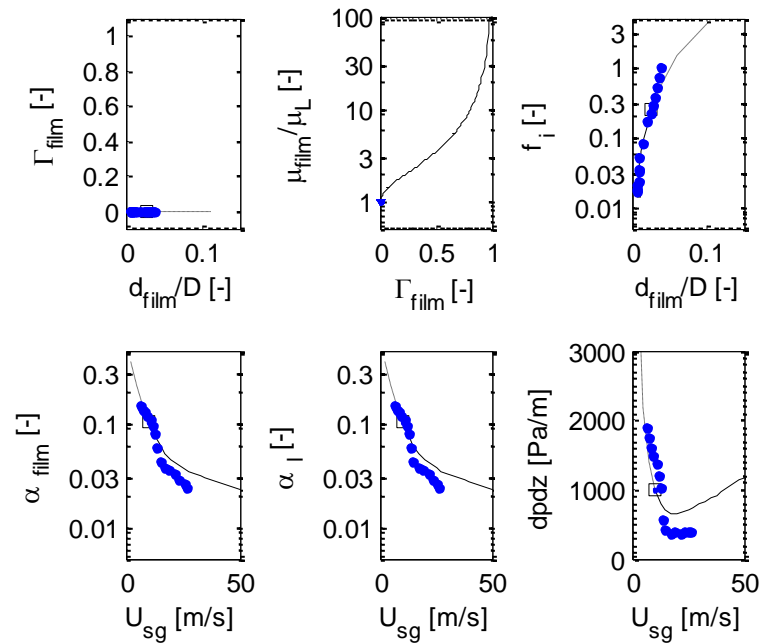
#	U_{sg} (m/s)	dp/dz (Pa/m)	α_f (-)	α_L (-)
<u>10.01</u>	9.64	1409.2	0.1251	0.1251
10.02	11.78	1255.2	0.0962	0.0962
10.03	14.98	1063.8	0.0572	0.0572
10.04	18.20	963.9	0.0390	0.0390
10.05	21.42	947.3	0.0296	0.0296
10.06	25.70	993.1	0.0334	0.0334
10.07	29.98	1080.4	0.0317	0.0317
10.08	34.26	1176.1	0.0279	0.0279
10.09	38.57	1305.1	0.0237	0.0237
10.10	42.87	1409.2	0.0211	0.0211

C.12 Set #11

Figure C.12 $D = 80 \text{ mm}$, $U_{\text{sl}} = 10 \text{ mm/s}$, $C = 0 \text{ ppm}$, Nimwegen (2015)Table C.12 $D = 80 \text{ mm}$, $U_{\text{sl}} = 10 \text{ mm/s}$, $C = 0 \text{ ppm}$, Nimwegen (2015)

#	U_{sg} (m/s)	dp/dz (Pa/m)	α_f (-)	α_L (-)
11.01	4.28	1881.9	0.1717	0.1717
11.02	6.43	1620.1	0.1412	0.1412
11.03	8.57	1229.3	0.1009	0.1009
11.04	10.75	<u>741.1</u>	0.0733	0.0733
<u>11.05</u>	12.85	271.9	0.0402	0.0402
<u>11.06</u>	15.01	289.2	0.0292	0.0292
<u>11.07</u>	17.18	252.0	0.0271	0.0271
11.08	19.29	252.4	0.0237	0.0237
11.09	21.42	273.6	0.0224	0.0224
11.10	23.59	282.3	0.0194	0.0194
11.11	25.72	295.2	0.0169	0.0169
11.12	27.87	316.4	0.0160	0.0160

C.13 Set #12

Figure C.13 $D = 80$ mm, $U_{sl} = 50$ mm/s, $C = 0$ ppm, Nimwegen (2015)Table C.13 $D = 80$ mm, $U_{sl} = 50$ mm/s, $C = 0$ ppm, Nimwegen (2015)

#	U_{sg} (m/s)	dp/dz (Pa/m)	α_f (-)	α_L (-)
12.01	6.42	1880.6	0.1480	0.1480
12.02	7.49	1743.3	0.1378	0.1378
12.03	8.57	1605.9	0.1289	0.1289
12.04	9.64	1476.9	0.1183	0.1183
12.05	10.74	1356.2	0.1068	0.1068
12.06	11.79	1185.5	0.0958	0.0958
12.07	12.85	1019.0	0.0801	0.0801
<u>12.08</u>	13.92	556.8	0.0593	0.0593
<u>12.09</u>	15.00	411.2	0.0419	0.0419
<u>12.10</u>	17.15	357.1	0.0373	0.0373
12.11	19.28	403.0	0.0351	0.0351
12.12	21.43	373.9	0.0322	0.0322
12.13	23.58	382.2	0.0292	0.0292
12.14	25.71	390.6	0.0258	0.0258
12.15	26.78	394.8	0.0237	0.0237

C.14 Set #13

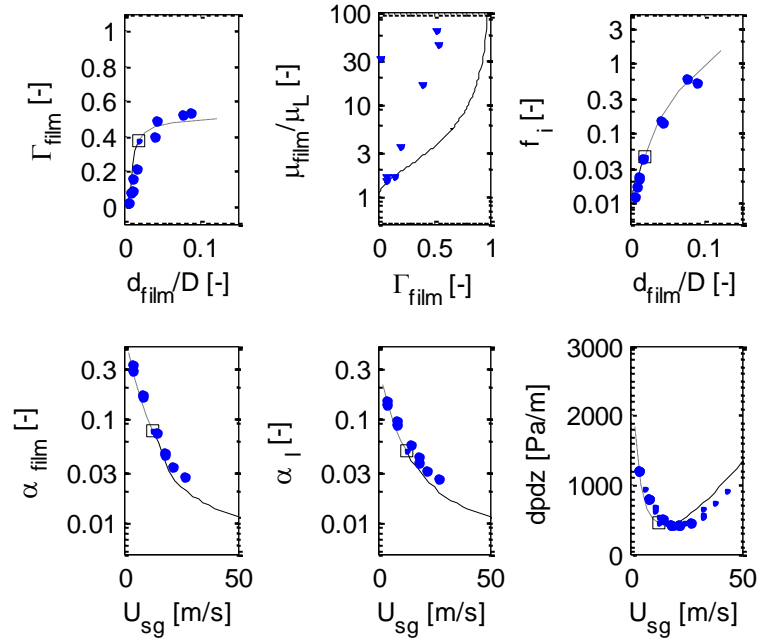
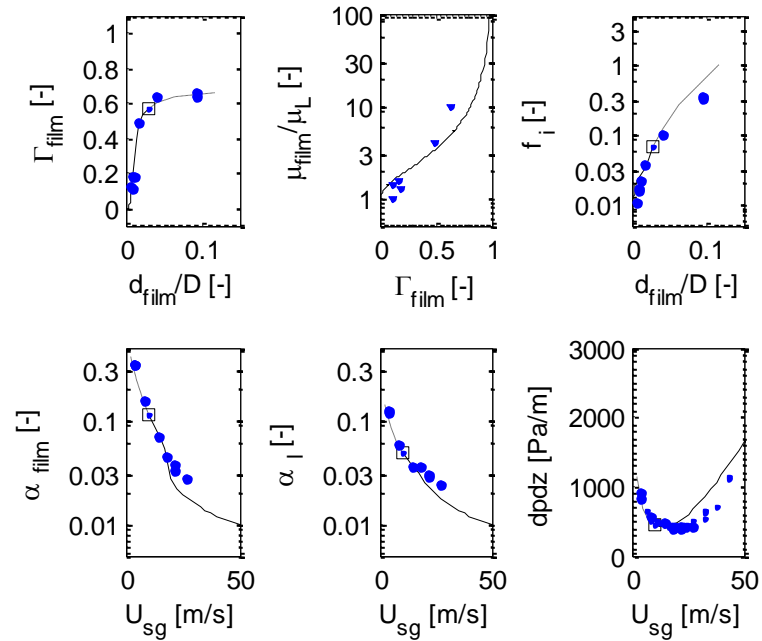


Figure C.14 $D = 50$ mm, $U_{sl} = 10$ mm/s, $C = 200$ ppm, TNO (2015)

Table C.14 $D = 50$ mm, $U_{sl} = 10$ mm/s, $C = 200$ ppm, TNO (2015)

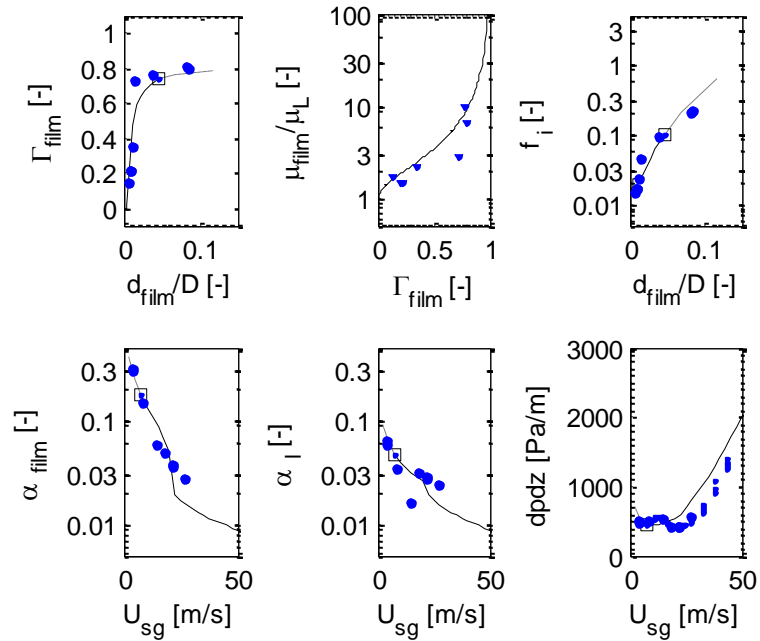
#	U_{sg} (m/s)	dp/dz (Pa/m)	α_f (-)	α_L (-)
<u>13.01</u>	4.29	1209.7	0.3240	0.1504
<u>13.02</u>	4.29	1182.9	0.2856	0.1356
<u>13.03</u>	8.59	807.0	0.1593	0.0952
<u>13.04</u>	8.59	784.5	0.1669	0.0852
<u>13.05</u>	14.49	510.0	0.0713	0.0563
<u>13.06</u>	18.25	422.8	0.0470	0.0429
13.07	18.25	406.9	0.0448	0.0377
13.08	21.47	428.4	0.0336	0.0312
13.09	26.83	452.1	0.0274	0.0268

C.15 Set #14

Figure C.15 $D = 50$ mm, $U_{\text{sl}} = 10$ mm/s, $C = 500$ ppm, TNO (2015)Table C.15 $D = 50$ mm, $U_{\text{sl}} = 10$ mm/s, $C = 500$ ppm, TNO (2015)

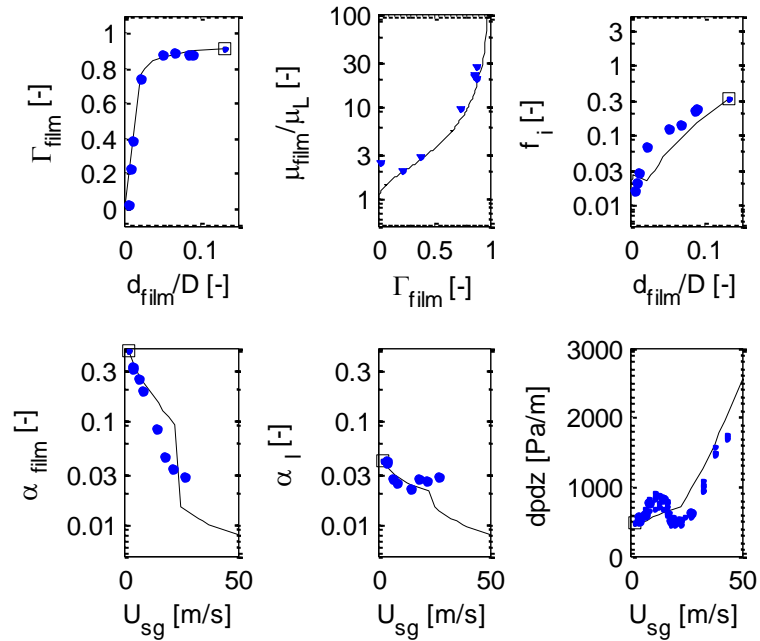
#	U_{sg} (m/s)	dp/dz (Pa/m)	α_f (-)	α_L (-)
<u>14.01</u>	4.29	915.3	0.3418	0.1256
<u>14.02</u>	4.29	821.5	0.3407	0.1164
<u>14.03</u>	8.59	554.9	0.1577	0.0581
14.04	14.49	472.5	0.0693	0.0355
14.05	18.25	402.4	0.0438	0.0361
14.06	21.47	386.7	0.0371	0.0304
14.07	21.47	427.0	0.0330	0.0292
14.08	26.83	404.8	0.0275	0.0243

C.16 Set #15

Figure C.16 $D = 50$ mm, $U_{sl} = 10$ mm/s, $C = 1000$ ppm, TNO (2015)Table C.16 $D = 50$ mm, $U_{sl} = 10$ mm/s, $C = 1000$ ppm, TNO (2015)

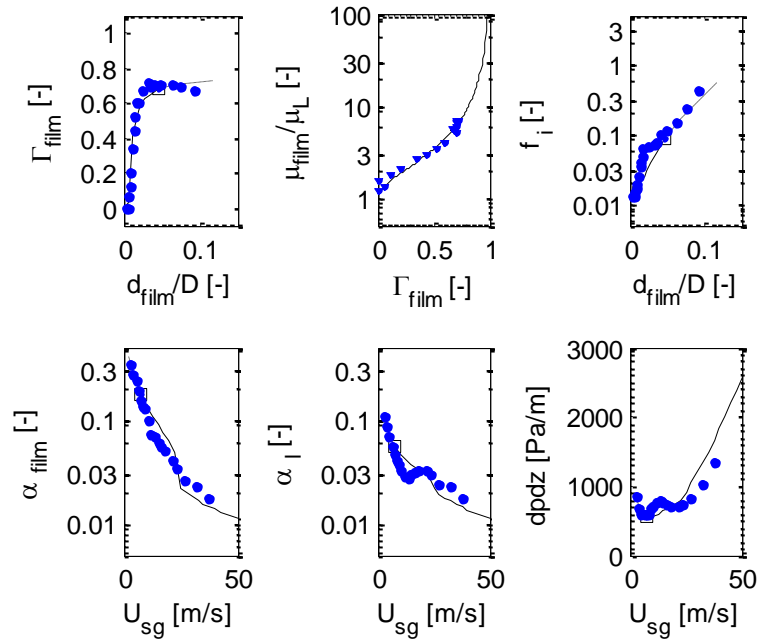
#	U_{sg} (m/s)	dp/dz (Pa/m)	α_f (-)	α_L (-)
<u>15.01</u>	4.29	474.9	0.3037	0.0596
<u>15.02</u>	4.29	510.6	0.3112	0.0629
15.03	8.59	508.5	0.1480	0.0343
15.04	14.49	533.5	0.0589	0.0161
15.05	18.25	428.3	0.0481	0.0311
15.06	21.47	418.1	0.0358	0.0280
15.07	21.47	410.5	0.0367	0.0291
15.08	26.83	551.5	0.0275	0.0236

C.17 Set #16

Figure C.17 $D = 50$ mm, $U_{sl} = 10$ mm/s, $C = 2000$ ppm, TNO (2015)Table C.17 $D = 50$ mm, $U_{sl} = 10$ mm/s, $C = 2000$ ppm, TNO (2015)

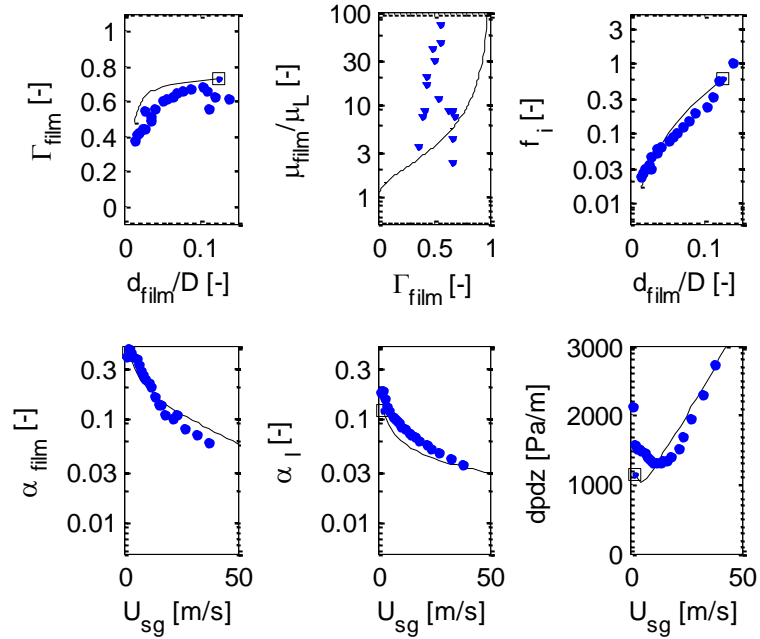
#	U_{sg} (m/s)	dp/dz (Pa/m)	α_f (-)	α_L (-)
16.01	4.29	575.8	0.3287	0.0401
16.02	4.29	518.3	0.3151	0.0401
16.03	6.44	587.3	0.2523	0.0278
16.04	8.59	767.5	0.1961	0.0251
16.05	14.49	834.5	0.0843	0.0219
16.06	18.25	510.8	0.0448	0.0275
16.07	21.47	510.7	0.0336	0.0259
16.08	26.83	615.5	0.0288	0.0282

C.18 Set #17

Figure C.18 $D = 34$ mm, $U_{sl} = 10$ mm/s, $C = 1000$ ppm, Nimwegen (2015)Table C.18 $D = 34$ mm, $U_{sl} = 10$ mm/s, $C = 1000$ ppm, Nimwegen (2015)

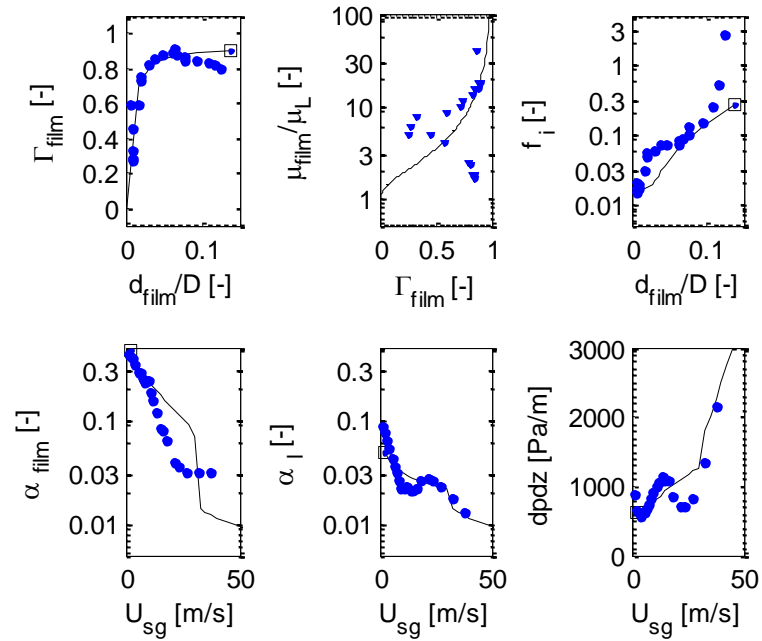
#	U_{sg} (m/s)	dp/dz (Pa/m)	α_f (-)	α_L (-)
<u>17.01</u>	3.20	840.0	0.3370	0.1102
<u>17.02</u>	4.28	685.2	<u>0.2780</u>	0.0853
<u>17.03</u>	5.33	597.4	0.2372	0.0708
17.04	6.41	580.9	<u>0.1898</u>	0.0567
17.05	7.47	602.2	0.1564	0.0463
17.06	8.55	598.1	<u>0.1347</u>	0.0409
17.07	9.64	678.0	0.1315	0.0370
17.08	10.70	720.1	<u>0.1003</u>	0.0327
17.09	11.78	753.9	0.0724	0.0285
17.10	13.93	791.8	<u>0.0698</u>	0.0276
17.11	15.05	<u>755.5</u>	0.0616	<u>0.0296</u>
17.12	16.08	729.0	<u>0.0559</u>	0.0310
17.13	18.22	695.6	0.0508	0.0332
17.14	21.43	704.4	0.0408	0.0324
17.15	23.57	734.0	0.0341	0.0299
17.16	26.79	822.5	0.0258	0.0240
17.17	32.15	1016.0	0.0233	0.0233
17.18	37.51	1327.0	0.0175	0.0175

C.19 Set #18

Figure C.19 $D = 34$ mm, $U_{sl} = 50$ mm/s, $C = 1000$ ppm, Nimwegen (2015)Table C.19 $D = 34$ mm, $U_{sl} = 50$ mm/s, $C = 1000$ ppm, Nimwegen (2015)

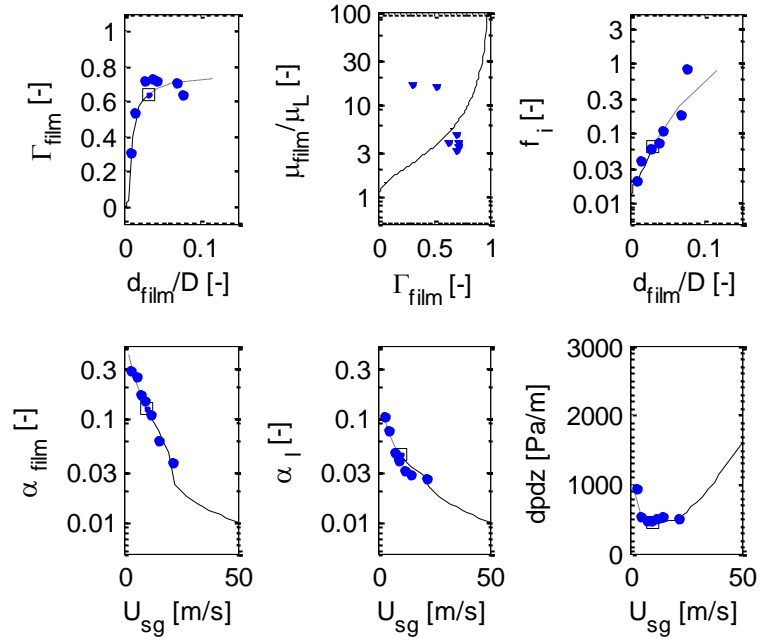
#	U_{sg} (m/s)	dp/dz (Pa/m)	α_f (-)	α_L (-)
18.01	1.07	2113.1	0.3978	0.1742
<u>18.02</u>	2.11	1581.0	0.4760	0.1856
<u>18.03</u>	3.20	1526.5	0.4194	0.1551
18.04	4.30	1505.6	<u>0.3917</u>	0.1310
18.05	5.34	1488.8	0.3728	0.1179
18.06	6.43	1455.3	<u>0.3221</u>	0.1058
18.07	7.52	1396.6	0.2904	0.0975
18.08	8.59	1363.1	<u>0.2633</u>	0.0930
18.09	9.63	1329.6	0.2397	0.0899
18.10	10.69	1312.8	<u>0.2160</u>	0.0844
18.11	11.81	1304.5	0.1989	0.0785
18.12	13.92	1308.7	<u>0.1613</u>	0.0716
18.13	15.03	<u>1334.9</u>	0.1365	0.0692
18.14	16.08	1350.6	<u>0.1350</u>	0.0661
18.15	18.23	1405.0	0.1082	0.0608
18.16	21.46	1518.2	0.0999	0.0553
18.17	23.59	1673.2	0.1107	0.0507
18.18	26.82	1937.1	0.0807	0.0469
18.19	32.18	2305.9	0.0691	0.0410
18.20	37.54	2720.7	0.0583	0.0364

C.20 Set #19

Figure C.20D = 34 mm, $U_{sl} = 10$ mm/s, $C = 3000$ ppm, Nimwegen (2015)Table C.20 D = 34 mm, $U_{sl} = 10$ mm/s, $C = 3000$ ppm, Nimwegen (2015)

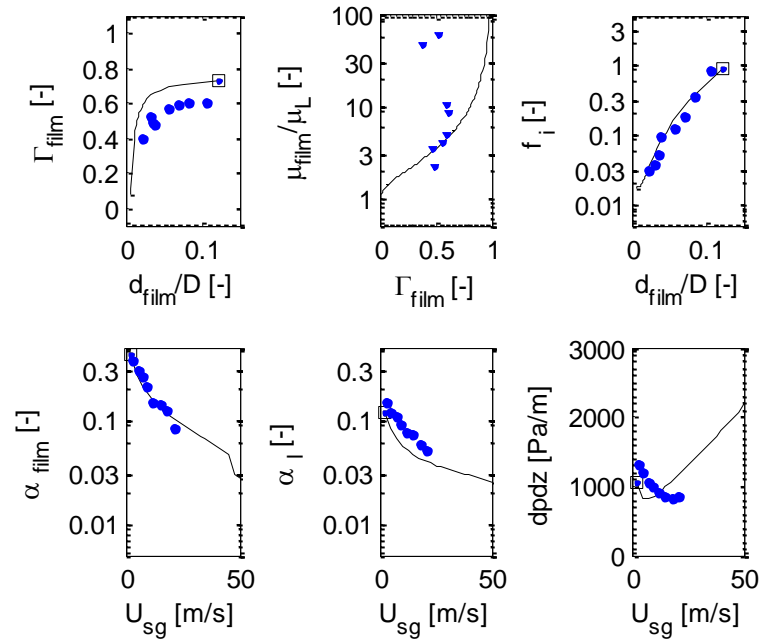
#	U_{sg} (m/s)	dp/dz (Pa/m)	α_f (-)	α_L (-)
19.01	1.06	886.3	0.4344	0.0877
<u>19.02</u>	2.13	651.6	0.4153	0.0767
<u>19.03</u>	3.21	630.9	0.3870	0.0644
19.04	4.26	555.6	<u>0.3420</u>	0.0524
19.05	5.36	610.4	0.2838	0.0433
19.06	6.41	665.1	<u>0.2844</u>	0.0366
19.07	7.49	745.0	0.2505	0.0319
19.08	8.55	833.3	<u>0.2323</u>	0.0259
19.09	9.66	917.4	0.2380	0.0221
19.10	10.73	993.0	<u>0.1826</u>	0.0216
19.11	11.80	1056.0	0.1515	0.0226
19.12	13.93	1144.4	<u>0.1170</u>	0.0208
19.13	15.00	<u>1086.7</u>	0.0824	0.0209
19.14	16.09	1069.0	<u>0.0801</u>	0.0216
19.15	18.21	838.4	0.0641	0.0260
19.16	21.45	708.6	0.0399	0.0269
19.17	23.58	717.2	0.0362	0.0261
19.18	26.80	826.7	0.0316	0.0232
19.19	32.17	1334.9	0.0316	0.0173
19.20	37.52	2157.9	0.0308	0.0127

C.21 Set #20

Figure C.21 $D = 50$ mm, $U_{sl} = 10$ mm/s, $C = 1000$ ppm, Nimwegen (2015)Table C.21 $D = 50$ mm, $U_{sl} = 10$ mm/s, $C = 1000$ ppm, Nimwegen (2015)

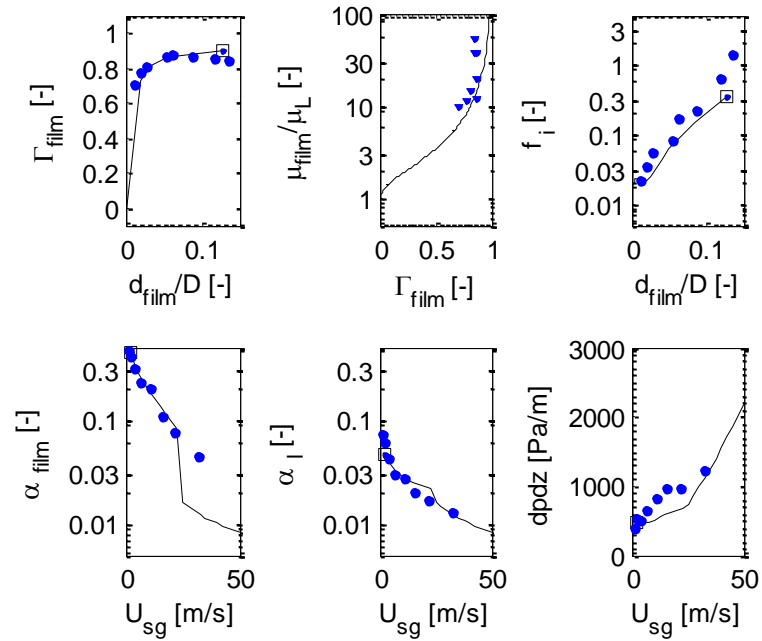
#	U_{sg} (m/s)	dp/dz (Pa/m)	α_f (-)	α_L (-)
<u>20.01</u>	3.22	950.6	0.2854	0.1026
<u>20.02</u>	5.34	530.2	0.2563	0.0746
20.03	7.50	476.4	0.1681	0.0467
20.04	9.62	476.8	0.1448	0.0395
20.05	11.79	518.8	0.1082	0.0311
20.06	14.99	523.6	0.0616	0.0290
20.07	21.44	504.0	0.0383	0.0265

C.22 Set #21

Figure C.22 $D = 50 \text{ mm}$, $U_{\text{sl}} = 50 \text{ mm/s}$, $C = 1000 \text{ ppm}$, Nimwegen (2015)Table C.22 $D = 50 \text{ mm}$, $U_{\text{sl}} = 50 \text{ mm/s}$, $C = 1000 \text{ ppm}$, Nimwegen (2015)

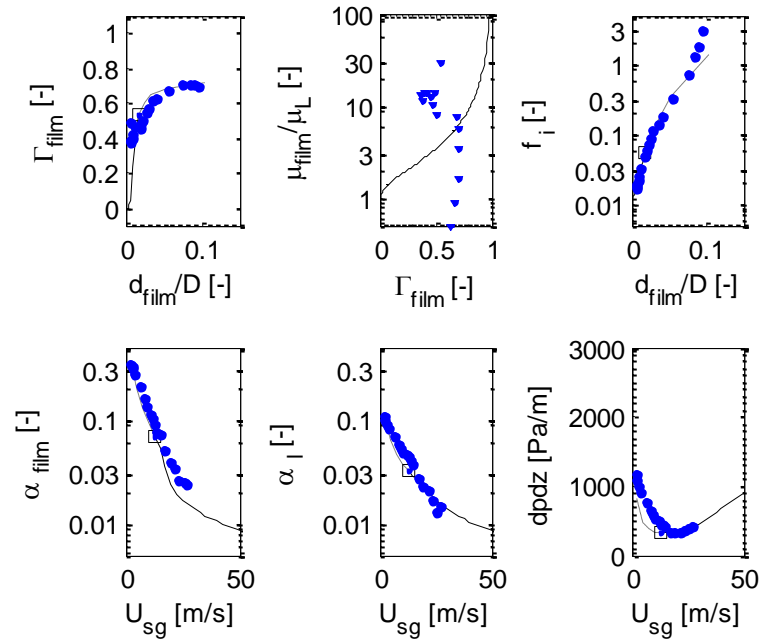
#	U_{sg} (m/s)	dp/dz (Pa/m)	α_f (-)	α_L (-)
<u>21.01</u>	3.17	1321.8	0.3811	0.1500
21.02	5.33	1184.5	0.3054	0.1195
<u>21.03</u>	7.50	1055.5	0.2630	0.1077
21.04	9.64	988.9	0.2130	0.0925
21.05	11.78	905.7	0.1456	0.0760
21.06	14.98	847.4	0.1406	0.0713
21.07	18.20	830.8	0.1240	0.0587
21.08	21.42	843.3	0.0840	0.0511

C.23 Set #22

Figure C.23 $D = 50$ mm, $U_{\text{sl}} = 10$ mm/s, $C = 3000$ ppm, Nimwegen (2015)Table C.23 $D = 50$ mm, $U_{\text{sl}} = 10$ mm/s, $C = 3000$ ppm, Nimwegen (2015)

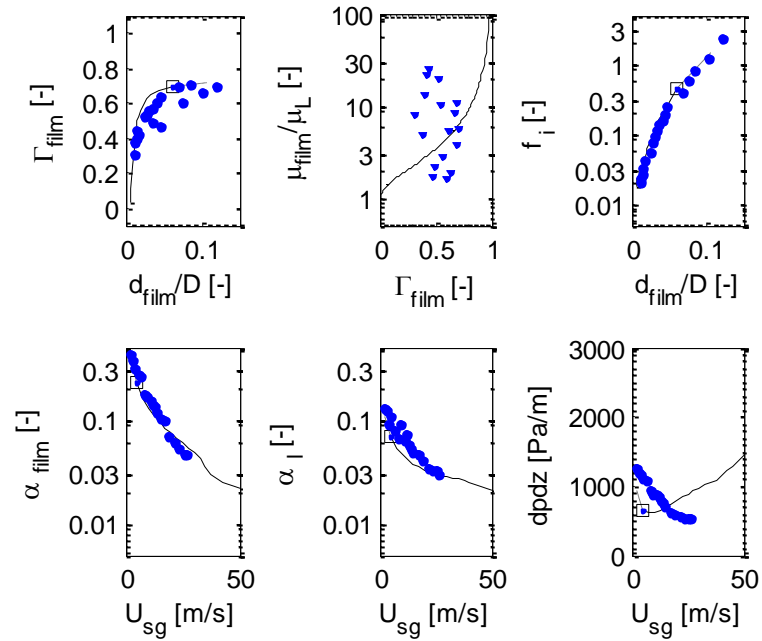
#	U_{sg} (m/s)	dp/dz (Pa/m)	α_f (-)	α_L (-)
<u>22.01</u>	1.06	387.7	0.4710	0.0742
<u>22.02</u>	2.14	525.4	0.4161	0.0619
22.03	4.28	509.1	0.3187	0.0424
22.04	6.42	642.9	0.2330	0.0297
22.05	10.72	818.7	0.2031	0.0277
22.06	16.06	953.0	0.1098	0.0205
22.07	21.43	958.1	0.0757	0.0168
22.08	32.16	1226.8	0.0441	0.0131

C.24 Set #23

Figure C.24 $D = 80$ mm, $U_{sl} = 10$ mm/s, $C = 1000$ ppm, Nimwegen (2015)Table C.24 $D = 80$ mm, $U_{sl} = 10$ mm/s, $C = 1000$ ppm, Nimwegen (2015)

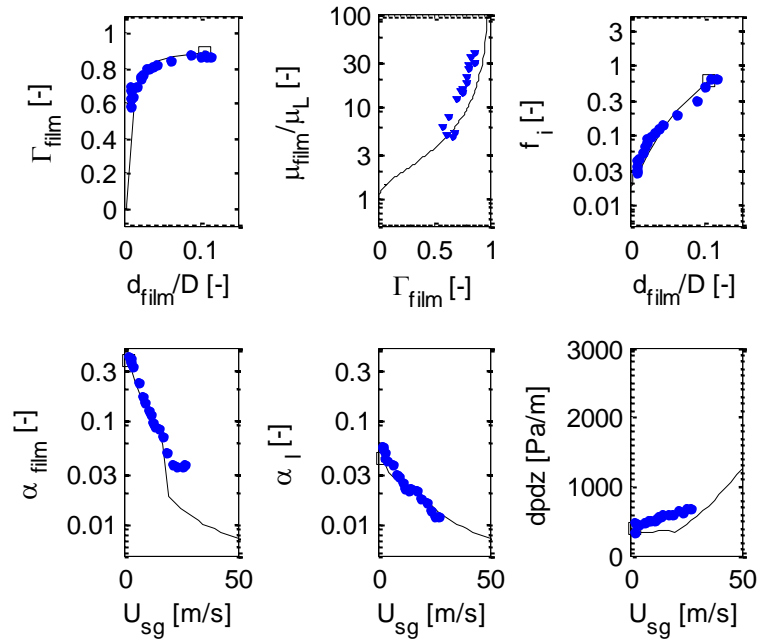
#	U_{sg} (m/s)	dp/dz (Pa/m)	α_f (-)	α_L (-)
23.01	2.12	1182.4	0.3470	0.1072
23.02	2.68	1086.7	<u>0.3298</u>	0.0988
23.03	3.20	1007.7	<u>0.3105</u>	0.0920
23.04	4.28	899.6	0.2796	0.0814
23.05	6.42	754.3	0.2089	0.0683
23.06	8.58	638.0	0.1589	0.0594
23.07	9.65	584.0	<u>0.1378</u>	0.0538
23.08	10.71	530.1	0.1132	0.0493
23.09	11.80	501.1	<u>0.1028</u>	0.0466
23.10	12.86	459.6	0.0899	0.0446
23.11	13.93	434.7	<u>0.0768</u>	0.0415
23.12	15.01	405.8	0.0724	0.0379
23.13	17.16	331.3	0.0516	0.0277
23.14	19.31	319.2	0.0391	0.0227
23.15	21.44	336.2	0.0350	0.0210
23.16	23.57	357.5	0.0266	0.0168
23.17	25.74	391.3	<u>0.0253</u>	0.0131
23.18	26.80	<u>405.1</u>	0.0241	0.0147

C.25 Set #24

Figure C.25 $D = 80$ mm, $U_{sl} = 50$ mm/s, $C = 1000$ ppm, Nimwegen (2015)Table C.25 $D = 80$ mm, $U_{sl} = 50$ mm/s, $C = 1000$ ppm, Nimwegen (2015)

#	U_{sg} (m/s)	dp/dz (Pa/m)	α_f (-)	α_L (-)
<u>24.01</u>	2.12	1264.0	0.4244	0.1293
<u>24.02</u>	3.19	1185.1	<u>0.3674</u>	0.1229
24.03	4.27	1172.8	0.3104	0.0924
24.04	5.36	1122.8	<u>0.2779</u>	0.1089
24.05	6.42	1068.7	0.2588	0.0802
24.06	8.57	939.6	0.1798	0.0653
<u>24.07</u>	9.64	893.9	<u>0.1727</u>	0.0924
24.08	10.74	877.3	0.1573	0.0624
24.09	11.79	840.0	<u>0.1418</u>	0.0720
24.10	12.85	802.7	0.1331	0.0582
24.11	13.92	761.1	<u>0.1189</u>	0.0529
24.12	15.00	711.1	0.1057	0.0489
24.13	17.15	632.0	0.0974	0.0464
24.14	19.28	590.4	0.0707	0.0409
24.15	21.43	553.0	0.0599	0.0337
24.16	23.58	528.0	0.0541	0.0325
24.17	25.71	519.7	<u>0.0466</u>	0.0322
24.18	26.78	523.9	0.0474	0.0295

C.26 Set #25

Figure C.26 $D = 80$ mm, $U_{sl} = 10$ mm/s, $C = 3000$ ppm, Nimwegen (2015)Table C.26 $D = 80$ mm, $U_{sl} = 10$ mm/s, $C = 3000$ ppm, Nimwegen (2015)

#	U_{sg} (m/s)	dp/dz (Pa/m)	α_f (-)	α_L (-)
<u>25.01</u>	2.15	328.4	0.4078	0.0555
<u>25.02</u>	2.68	478.7	<u>0.3865</u>	0.0534
<u>25.03</u>	3.20	458.1	<u>0.3605</u>	0.0500
25.04	4.28	450.1	0.3254	0.0407
25.05	6.42	475.9	0.2330	0.0378
25.06	8.58	509.4	0.1656	0.0302
25.07	9.63	518.0	<u>0.1500</u>	0.0283
25.08	10.71	518.2	0.1248	0.0255
25.09	11.80	539.3	<u>0.1125</u>	0.0224
25.10	12.86	552.0	0.0932	0.0217
25.11	13.93	564.6	<u>0.0861</u>	0.0211
25.12	15.01	577.3	0.0832	0.0218
25.13	17.15	594.3	0.0691	0.0209
25.14	19.29	603.0	0.0491	0.0180
25.15	21.44	649.3	0.0374	0.0159
25.16	23.58	633.0	0.0366	0.0138
25.17	25.72	670.9	<u>0.0365</u>	0.0118
25.18	26.80	<u>690.9</u>	0.0383	0.0117

D Rheology of foams

D.1 Introduction

As indicated in section 3.4.2 there are two reasons to study the rheology of foams.

1. Find out if the film model predictions are best by using the viscosity closure model of Mitchell (eq. 3.13) or by determining experimentally the relation between viscosity and foam quality.
2. Investigate the possibility to retrieve properties from rheological measurements that can be related to the performance of the surfactants in practice.

The first subject is treated in paragraph 3.4.2. In this Appendix we First give some more background on rheological measurements

Then we will describe the development of the measurements of the rheological properties of foam. As already indicated it is very important to choose the conditions for the determination of the properties foam as it is a structured material and at the same time foams change in time due to drainage in case of dry foams and due to buoyancy of bubbles in case of wet foams.

Next the experimental results are given and it is indicated how this types of measurement can contribute to the evaluation of surfactants and prediction of their efficacy.

D.2 General background rheology

The viscoelastic behaviour can be studied by rheological measurements. The technical definition of rheology is 'the science of deformation & flow' but what does it (really) mean ?

When a solid is stressed it deforms, and when a liquid is stressed it flows. When an ideal solid is deformed it will go back to its original state after the stress is released. So all energy we put in to deform it, is stored in the structure and used for relaxation. When an ideal liquid is stressed, the molecules are allowed to flow over each other. This process generates friction and consequently some heat and this heat will be lost to the environment. The energy that is put in is used up, the liquid will not return to the original state.

Materials with a complex internal structure can show both solid like and liquid like behaviour. The materials that behave in between the ideal liquids and ideal solids are said to show visco-elastic behaviour. Rheology primarily describes the behaviour of complex materials.

Configurations

To study rheology of a liquid we apply a controlled stress (torque of the rheometer over a known geometry surface) and measure the speed of the movement.

A number of configurations with well-defined design are used. The configuration is chosen based on the application and range of expected values for the viscosity and the texture of the material.

The most used configurations are given in Figure D.1. The cone plate configuration gives a deformation that is the same over the whole surface from the middle to the outer rim but can only be used for completely homogeneous samples. The deformation is less well defined but is more broadly applicable. The concentric cylinder configuration is the most versatile and allows many variations in configuration and consistency of the sample. The double-gap configuration is used for low viscous samples that need a large measuring surface and small gap.

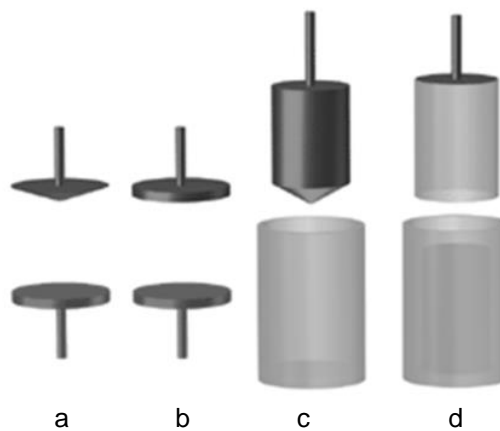


Figure D.1: Widely used configurations in rheology measurements: cone-plate (a), plate-plate (b), concentric cylinders (c) and double gap (d).

To determine the viscosity of liquids an alternative that is often used is to study the flow in a narrow pipe or tube. In general the pressure drop between two points is measured as a function of the flow of the liquid that is imposed or alternatively the flow is measured caused by a given pressure difference. For these measurements assumptions need to be made about the flow regime in the pipe and wall effects need to be considered. For structured materials like foams this is not straightforward. For foams also the compressibility need to be taken into account. As example the closure relation used in the modelling was established based on this type of measurement (ref. Mitchell). As argued these measurements do not tell the whole story and cannot be used to describe the different phenomena observed and is therefore not considered here.

The cone-plate, plate-plate and double gap configurations have by definition a small gap between the two surfaces. Therefore, in these configurations it is not possible to accommodate a layer with a thickness of more than a few bubbles and wall effects will be dominant. As a consequence it is chosen to use a configuration based on concentric cylinders.

Measuring mode: Rotation vs. Oscillation

There are two main modes to execute rheological measurements: in rotation and in oscillation (See figure below).

In *rotation* the measurement is performed under a constant rotational shear rate and the shear stress is measured or the other way around. This gives a straightforward value of the viscosity.

Things to consider:

- The material is regarded to be purely viscous and any elasticity in the structure is neglected.
- The sample is under continuous flow and in case of structured materials like foam the structure will be different than structure of the foam in conditions without flow and will depend on the shear rate applied.
- In this mode the situation is very similar to the situation in a foam film in a liquid loading situation. Therefore this type of measurements were used to generate viscosity values to evaluate the TPC modelling.

In general when we want to determine the visco-elastic behaviour of a structured material, we want to keep the structure intact. Therefore, very small deformations are applied in the form of small amplitude *oscillations*. So rather than applying a constant shear stress or shear rate we deform the material with small amplitude in one direction and going back and forth as shown schematically in figure D.2 and apply a sinusoidal stress or strain. If a given oscillatory strain is applied the stress is measured and vice versa. Above a give stress (amplitude) of the oscillation, the structure will be influenced and change or completely break down. The point at which the structure starts to change is also a characteristics of a material. In the case of a foam it is also an indication of the strength of the lamella that are present in the foam and therefore an indication for the stability of the foam.

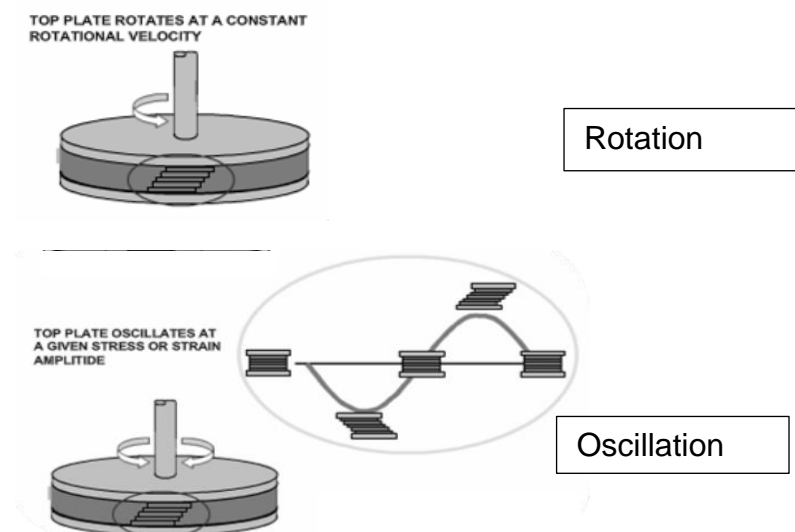


Figure D.2: Schematic representation of measurement rotational and oscillatory modes for study of viscosity and visco-elastic behaviour.

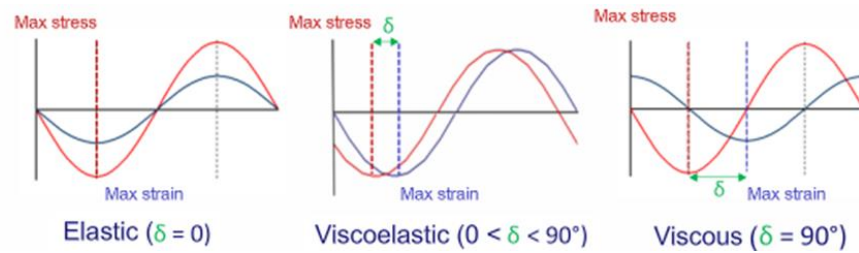


Figure D.3: Relation between stress and strain in rheological measurements for liquids (viscous) and solids (elastic) and materials with complex behaviour (visco-elastic). δ is phase lag between strain and stress.

The interpretation of oscillation measurements is not as straightforward as for measurements in rotation.

From the oscillations we can calculate various parameters like the complex modulus G^* . That is a measure of the overall material stiffness with contributions from viscous and elastic elements. G^* is defined as the ratio between the maximum stress and the maximum strain.

When a strain is applied and a stress is measured, there is a phase lag observed. This time lag depends on the material properties. For a purely elastic material (solid behaviour), the stress is in phase with the strain and there is no phase lag. For a pure viscous (liquid behaviour), the phase lag is 90° . For a visco-elastic material the phase lag is somewhere in between. Therefore, the phase angle is another important property that is used to understand the material's behaviour. It allows to break down the G^* into its component parts:

Storage (elastic) modulus given by $G' = G^* \cos\delta$

and

Loss (viscous) modulus given by $G'' = G^* \sin\delta$

The breakdown of G^* in components can be represented in a vector representation as in the figure below.

This means that if $G' > G''$ the material has more a solid character, while for $G'' > G'$ the material has a more liquid character. Based on this more information about the structure and the dependence of the structure on various conditions can be determined.

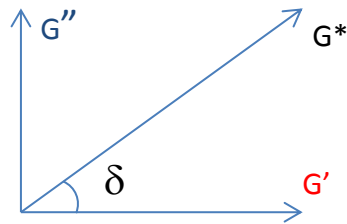


Figure D.4 Graphic representation of relation between storage modulus G' , Loss modulus G'' , Complex modulus G^* and the phase lag δ between strain and stress

From the complex modulus by dividing the modulus by the oscillation frequency:
 $\eta^* = G^*/\omega$.

D.3 Development experimental set-up to study rheology of foam

As indicated liquid foams are structured materials. Furthermore liquid foams are not stable in time. This means various parameters that play a non-negligible role and need to be controlled at the same time [19]. Important parameters are foam quality, i.e. gas volume fraction, foam texture (bubbles size distribution), size of the measurement apparatus compared to bubbles size, influence of foam production method, wall slip phenomena and foam compressibility. An important issue is also to keep the foam quality constant during the measurement.

Therefore, it is important to adapt the execution of the experiment to the conditions that are encountered in practice and to the information that we want to retrieve to obtain results that are relevant for the application.

A first step was to deal with the fact that foam is not stable. Dry foams show drainage and in wet foams the bubbles rise due to buoyancy. The approach that was chosen was to generate foam continuously and have it flow through the measuring setup. Also we wanted to have a measuring method where we could easily vary the quality/wetness of the foam.

To this end a predetermined flow of gas and of liquid are combined and pumped through the frit of a glass filter that functions as sparger. The flows of the gas and the liquid can be varied independently and in this way foams with different quality can be produced reproducibly as demonstrated in Figure D.5.

The size of the cup is chosen to allow the positioning of the rotor of the rheometer inside the glass cup of the filter. The cup in this way functions as the outer cylinder in concentric cylinder type of measurement. Another unconventional thing we did was not to use a solid cylinder as a rotor but to use a rotor with 4 vertical blades. As indicated the structure of foam close to the wall is different from the structure in bulk. It is known that wall effects play a role and is a cause for errors in the measurement. It is observed that during the rotation of the rotor the foam is trapped between the blades and hardly moves. In this way the blades and the foam more or

less behave like a foam cylinder that moves inside the outer cylinder. In this way most of the wall effects is expected to be avoided.

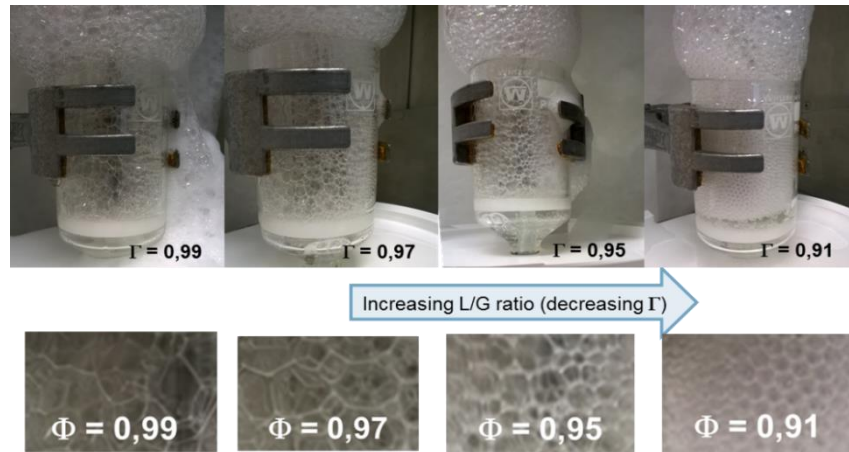


Figure D.5: Demonstration of generation of foam with different qualities.

A last an important aspect is that the distance between the rotor and the outer cylinder is large compared with the bubble making that during a measurement the properties of the foam as a whole are determined and not an individual layer of foam cells.

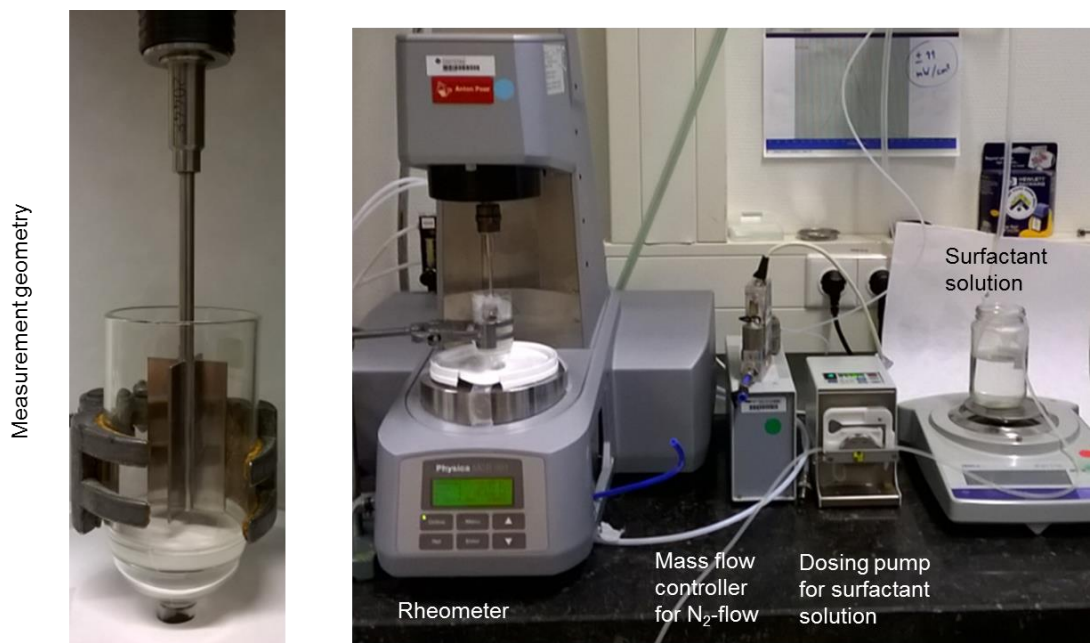


Figure D.6: Experimental set-up to measure rheological properties

First measurements with relatively dry foams were performed and stability of the foams in the measuring cup looked quite stable. Later it appeared that in the flow loop experiments mostly quite wet foams are present and we also need to look into the possibility to determine the rheology of wet foams. For wet foams (quality < 0.8) drainage rates are much higher and a little layer of liquid appeared at the bottom of

the measuring cup. To mitigate this drainage we added a polyethylene oxide (PEO) with a molar mass of 400kD. The amounts added were 1 % at the first set of experiments. Later it appeared that the addition of 0,25% was enough to suppress the drainage. Especially at 0,25 % the influence of the presence of the PEO is small. For comparison with outcome of flow loop experiments the slight increase of the viscosity of the liquid is accounted for.

The quality and wetness indicated in the graphs are calculated on the basis of the volume of the gas flow and the volume of the liquid flow. Late in the project we realised some liquid may build-up in the cup and some preliminary experiments indicate that this is indeed the case. This means that in the indicated qualities there is some overestimation and in practice the indicated qualities are lower than the ones calculated from the dosed gas and liquid flow. Some more experimental work would be needed to sort this out in more detail.

D.4 Experimental results

Determination yield point and flow point

First measurements were performed with high quality foams. The storage modulus and loss modulus were determined as a function of the amplitude of an oscillatory measurement. The frequency of the oscillation for all measurements is 1 Hz. In the figure below figure below the results are given for a foam with a quality of 90%. On the horizontal axis the amplitude of the oscillation is translated to the value of the maximum shear stress that occurs during the oscillation. In this way it gives a better idea about the values in the graph.

At very small shear stress (and amplitude) the storage modulus G' is a little higher than the loss modulus G'' . this means the foam behaves mainly as an elastic solid with some viscous flow as well. At a given amplitude that corresponds with a shear stress of 9 Pa, the storage modulus starts to drop meaning that the structure is disturbed. This is defined as the yield point and after this point the foam starts to show shear thinning behaviour. If the amplitude is further increased the storage modulus drops faster than the loss modulus and crosses the curve of the loss modulus at shear stress of 18 Pa. Beyond this point the foam behaves more like a liquid than like a solid. The cross-over point is defined as the flow point.

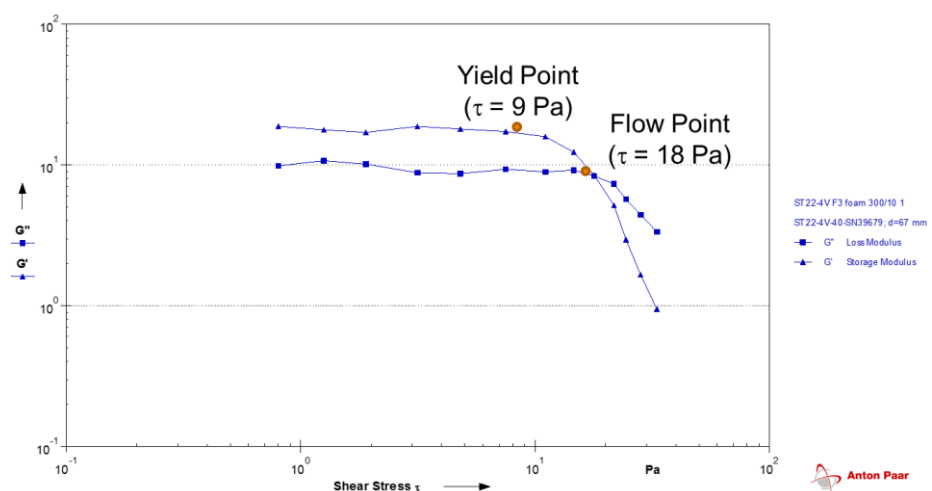


Figure D.6: loss modulus and storage modulus for a high quality foam

Influence foam quality

These measurements were next performed for a wide range of qualities between 91% and 62,5%. The foamer is Fomatron and the concentration is 750 ppm. To mitigate the drainage 1% PEO was added to the liquid. The results are given in figure D.7 In this case the horizontal axis is the imposed amplitude of the oscillation is given.

As both the storage and loss modulus are plotted for the different curves the figure is quite busy, but it allows a very nice comparison between the different qualities. The foam with a quality of 91% behave like the one we discussed in the previous figure. It starts off with a solid like behaviour at low amplitudes and ends up behaving like a liquid at high amplitudes. For the foam with a quality of 83,3% at low amplitudes the storage modulus is still a little higher than the loss modulus but they are closer together than for the 91% foam. The flow point is also situated at a lower amplitude of the deflection angle. For the quality of 76,9% the foam also at the low amplitudes behaves more like a liquid but with still a considerable amount of elastic contribution to the overall complex modulus. Already at 71,4% the contribution of the storage modulus becomes significantly lower and a little elasticity is left in the foam. For a quality of 62,5 %hardly any elasticity can be detected. The pink line is the loss modulus for liquid. The increase of the curve and the high amplitudes is due to turbulence effects observed for the low viscosity as also found for the measurements performed in rotation.

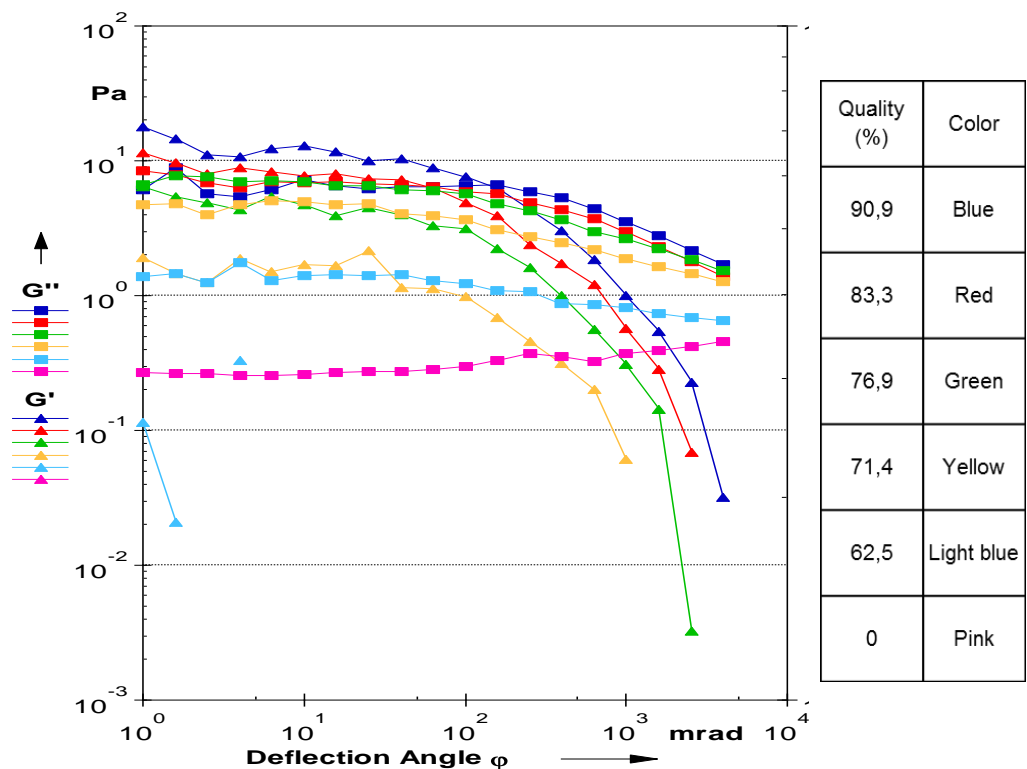


Figure D.7: Storage modulus and loss modulus for different foam qualities as function of amplitude of deflection angle. Concentration Fomatron: 750 ppm. 1% PEO in the liquid.

In Figure D.8 the same data are translated from storage and loss modulus to complex viscosity. Of course less information is available if just the viscosity is plotted, but these are the values needed if translation to process parameters. Since it is not so busy the figure more clearly shows the shear thinning behaviour of the foams and how this shear thinning behaviour changes with the foam quality. Foams with high quality show a higher shear thinning behaviour than the low quality foams. With the foam with 62,5 % almost behaving like a Newtonian liquid. Especially if we realise that the y-axis is logarithmic we see that the effects are very large. This same trend was also observed for the measurements performed in rotation as discussed in paragraph 3.4.2.

Further comparison of these oscillatory measurements with the measurements in rotation of paragraph 3.4.2 shows that in the rotation measurements no plateau is found at the low deformation rates. In the measurements the foam is forced to flow and behave like a liquid. So both measurement modes give complementary information about the nature and behaviour of the foam.

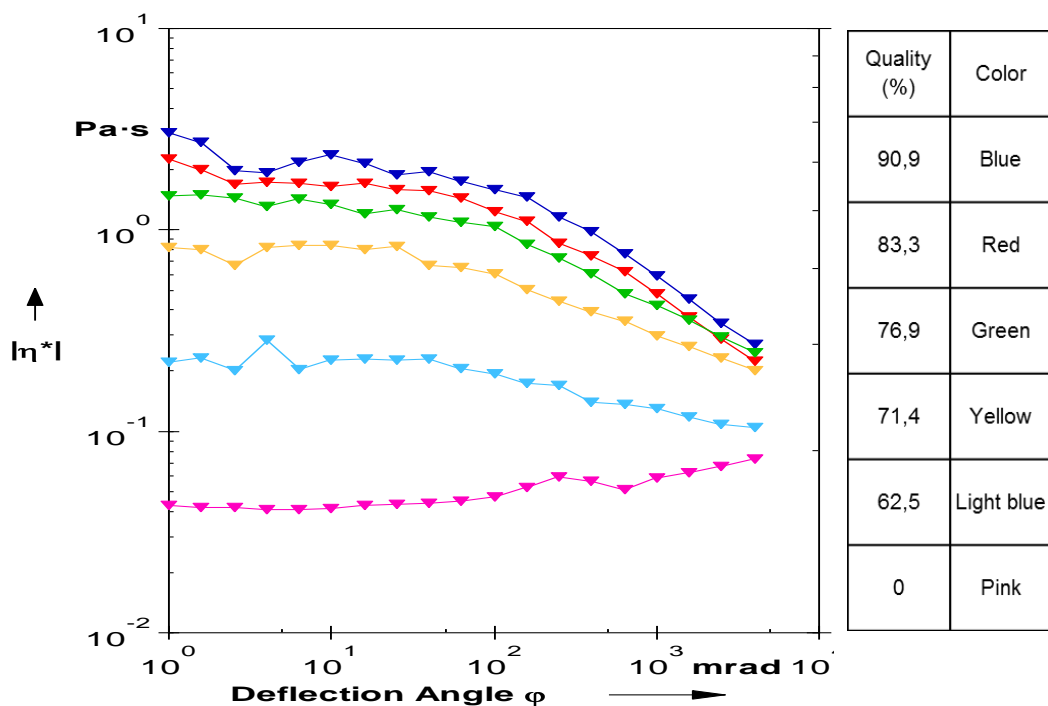


Figure D.8: Complex viscosity for different foam qualities as function of amplitude of deflection angle. Concentration Foamatron: 750 ppm. 1% polyethyleneoxide in the liquid.

Influence surfactant concentration

These measurements were further extended and these measurements were repeated for different surfactant concentrations. To be able to compare the results the complex viscosities are considered in the plateau area at low deformation.

These viscosities are plotted as a function of the wetness of the foam. First of all the S-shape shows that at high quality (low wetness) the viscosity is nearly constant. Below a quality of about 90% the viscosity starts to decrease and after a strong decrease in the quality range of 70% and 50% the decrease levels off as we approach a regime that is described better as bubbly flow than as a foam. Further it was quite surprising to see that the results for the different foamer concentration are close together.

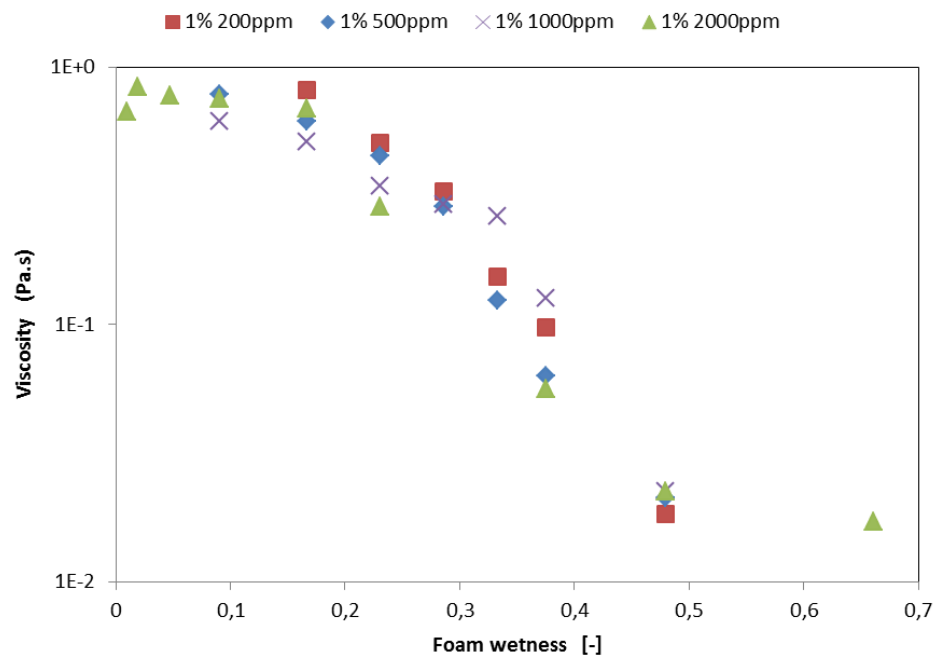


Figure D.9: Complex viscosity for different qualities calculated from the plateau at low amplitudes. Effect of foamer concentration. Foamer: Foamatron. Concentrations between 200ppm and 2000 ppm. Polyethyleneoxide concentration 1%.

This indicates that as soon as the amount of surfactant is high enough to stabilise the lamellae in the foam, the excess of foamer does not influence the intrinsic rheology of the foam at low deformations as such.

As soon as there are salts present and condensate/hydrocarbons it is expected that the situation will become different. Salts will reduce the effectiveness of the surfactants to form bubbles so the structure of the foam will be influenced. Condensates will be emulsified and this will also use-up foamer for the stabilisation of the emulsion. At considerable condensate concentrations the emulsified droplets will also influence the viscosity of the film and may even end up as a creamy substance. It would also be interesting to see how this translates to measurements in rotation as there the behaviour under flow and high shear are mimicked better.

D.5 Conclusion

Where do rheological data contribute?

To be able to see where the rheology data fit in the complete picture it is good to look at the mechanism of foam formation. There are there two conditions that need to be fulfilled to be able to generate a foam:

- gas bubbles need to be introduced in the liquid
- the bubbles need to have a significant lifetime

In the end the ratio between the number of bubbles formed and the number of bubbles destroyed will determine what the foam quality under a given condition will be.

To introduce gas bubbles into a liquid it is necessary that there is mechanical movement of the liquid e.g. in this case by breaking waves. This formation of breaking waves and the introduction formation of bubbles is facilitated by a reduction of the surface tension. A low surface tension also facilitates the formation of small bubbles.

In the flow loop experiments it is observed that at high gas velocities little to no foam is present even at high foamer concentration. The main reason is that at high gas velocities the flow is mainly co-annular laminar flow and only a limited amount of gas bubbles are introduced in the film.

A higher quality of foam is found at lower gas velocities especially if we get closer to the churn flow regime as there more breaking waves occur and more gas bubbles are introduced in the film.

Regarding the lifetime and stability of the foam bubbles depends of the strength of the foam lamellae. Mechanisms for destruction are: Two gas bubbles that collide and the film between them bursts or the bubbles ends-up at the film surface and there the foam lamella is destroyed. The foam lamella is either destroyed by drainage or by mechanical deformation. In our case drainage is expected to be too slow and mechanical deformation seems the most apparent mechanism. The strength of a foam lamella is largely determined by the specific foamer quality of the foamer formulation. It is not just surface tension but also stacking of the surfactant and effect of supporting actions of additives in the foamer like co-surfactants.

This means that there are three basic aspects that need to be understood to be able to predict the final behaviour:

- flow conditions
- surface activity of the liquid
- rheological properties of the foam.

Rheological properties on the one hand allow to quantification the flow properties of foams and on the other hand to the help to determine the sensitivity of the foam to mechanical deformation like shear forces. In this way it is related to the stability of foam (lifetime of the bubbles) in practical conditions. For this last aspect it is expected to be closely related to collapse tests.

Results realised in this work

- A relative simple experimental set-up is realised and was fit to an existing rheometer.
- Various important parameters are kept constant during the measurement

- The set-up allows the reproducible determination of important rheological characteristics of a foamer for a wide range of qualities and shear rates.
- Comparison of rotational measurements and measurements under oscillation contribute to the understanding of the rheological behaviour of foam.
- Measured values could be compared with values calculated from flow loop experiments. A hypothesis is that the film layer thickness influences the rheological behaviour and wall effects or restriction of bubbles size and movement in this layer may play a role in the performance.

Future work

The measurements allow the evaluation of the influence of a foamer on the structure of the foam and stability of the foam under shear conditions. This opens the possibility to evaluate in more depth the influence of different conditions like presence condensate and salt. The relation between the foamer performance and the influence on the foam structure under these conditions can be determined. In this way better understand the failure mechanisms under some conditions in practice or why certain foamers can cope with these conditions. The hypothesis of the influence of the layer thickness on the performance may be investigated further by studying the effect of the gap between the rotor and the outer cylinder.